



Final report on in-reactor uniaxial tensile deformation of pure iron and Fe-Cr alloy

Singh, Bachu Narain; Huang, X.; Tähtinen, S.; Moilanen, P.; Jacquet, P.; Dekeyser, J.

Publication date:
2007

Document Version
Publisher's PDF, also known as Version of record

[Link back to DTU Orbit](#)

Citation (APA):

Singh, B. N., Huang, X., Tähtinen, S., Moilanen, P., Jacquet, P., & Dekeyser, J. (2007). *Final report on in-reactor uniaxial tensile deformation of pure iron and Fe-Cr alloy*. Risø National Laboratory. Denmark. Forskningscenter Risø. Risøe-R No. 1616(EN)

General rights

Copyright and moral rights for the publications made accessible in the public portal are retained by the authors and/or other copyright owners and it is a condition of accessing publications that users recognise and abide by the legal requirements associated with these rights.

- Users may download and print one copy of any publication from the public portal for the purpose of private study or research.
- You may not further distribute the material or use it for any profit-making activity or commercial gain
- You may freely distribute the URL identifying the publication in the public portal

If you believe that this document breaches copyright please contact us providing details, and we will remove access to the work immediately and investigate your claim.

Final Report on In-reactor Uniaxial Tensile Deformation of Pure Iron and Fe-Cr Alloy

B. N. Singh, Xiaoxu Huang, S. Tähtinen, P. Moilanen, P.
Jacquet and J. Dekeyser

Risø-R-1616(EN)

Author: B. N. Singh ¹⁾, Xiaoxu Huang ¹⁾, S. Tähtinen ²⁾, P. Moilamen ²⁾, P. Jacquet ³⁾ and J. Dekeyser ³⁾

Title: Final Report on In-reactor Uniaxial Tensile Deformation of Pure Iron and Fe-Cr Alloy

Department: Materials Research Department

- ¹⁾ Materials Research Department,
Risø National Laboratory, DK-4000 Roskilde, Denmark
²⁾ VTT Industrial Systems, FIN-02044 VTT, Finland
³⁾ Reactor Technology Design Department, SCK•CEN, 200
Boeretang, B-2400 Mol, Belgium

Abstract :

Traditionally, the effect of irradiation on mechanical properties of metals and alloys is determined using post-irradiation tests carried out on pre-irradiated specimens and in the absence of irradiation environment. The results of these tests may not be representative of deformation behaviour of materials used in the structural components of a fission or fusion reactor where the materials will be exposed concurrently to displacement damage and external and/or internal stresses. In an effort to evaluate and understand the dynamic response of materials under these conditions, we have recently performed a series of uniaxial tensile tests on Fe-Cr and pure iron specimens in the BR-2 reactor at Mol (Belgium). The present report first provides a brief description of the test facilities and the procedure used for performing the in-reactor tests. The results on the mechanical response of materials during these tests are presented in the form of stress-displacement dose and the conventional stress-strain curves. For comparison, the results of post-irradiation tests and tests carried out on unirradiated specimens are also presented. Results of microstructural investigations on the unirradiated and deformed, irradiated and undeformed, post-irradiation deformed and the in-reactor deformed specimens are also described.

During the in-reactor tests the specimens of both Fe-Cr alloy and pure iron deform in a homogeneous manner and do not exhibit the phenomenon of yield drop. An increase in the pre-yield dose increases the yield stress but not the level of maximum flow stress during the in-reactor deformation of Fe-Cr alloy. Neither the in-reactor nor the post-irradiation deformed specimens of Fe-Cr alloy and pure iron showed any evidence of cleared channel formation. Both in Fe-Cr and pure iron, the in-reactor deformation leads to accumulation of dislocations in a homogeneous fashion and only to a modest density. No dislocation cells are formed during the in-reactor or post-irradiation deformation of Fe-Cr and pure iron.

Furthermore, in both cases, the slip systems even in the planes with Schmid factor value of almost zero get activated during the in-reactor as well as post-irradiation deformation. The main implications of these results are briefly discussed.

Risø-R-1616(EN)
November 2007

ISSN 0106-2840
ISBN 978-87-550-3620-8

Contract no.: TW5-
TTMS-007

Group's own reg. no.:
1610008-00

Sponsorship:
EU-Fusion Technology
Programme

Cover:

Pages: 52
Tables: 3
References: 14

Information Service Department
Risø National Laboratory
Technical University of Denmark
P.O.Box 49
DK-4000 Roskilde
Denmark
Telephone +45 46774004
bibl@risoe.dk
Fax +45 46774013
www.risoe.dk

Contents

1. Introduction	4
2. Materials and Experimental Procedure	5
2.1 Materials	5
2.2 Test module and irradiation rig	6
2.3 In- reactor uniaxial tensile tests	6
2.4 Microstructural investigations	8
3. Differences between post-irradiation and in-reactor tensile tests	8
3.1 Post-irradiation tensile tests	9
3.2 In-reactor tensile tests	10
4. Experimental Results	11
4.1 Mechanical response	11
4.2 Microstructural response	14
4.2.1 Dislocation microstructure in unirradiated and tensile tested specimens	15
4.2.2 Microstructure in the in-reactor tensile tested specimens	16
4.2.3 Microstructure of post-irradiation tensile tested specimens	19
5. Discussion	21
6. Summary and Conclusions	24
Acknowledgements	
References	
Figures	

1 Introduction

Effects of neutron irradiation on physical and mechanical properties of the low activation ferritic-martensitic steels are being extensively studied internationally since these alloys are considered to be leading candidate materials for the blanket and first wall of fusion reactors (e. g. DEMO) [1]. The ferritic-martensitic steels are also being considered to be leading candidate materials for the pressure vessels of recently proposed Generation IV fission reactors [2]. These alloys are considered to have a number of more attractive properties than alternative structural materials like ferritic and austenitic steels or vanadium alloys [2, 3]. These considerations have generated a considerable amount of international research activities to understand the effects of neutron irradiation on the physical and mechanical properties of ferritic-martensitic steels [4].

Although ferritic-martensitic steels are very resistant to swelling and maintain good fracture toughness at irradiation temperatures above about 673K [5], they are prone to loss of ductility at lower irradiation temperatures [6,7]. This so called “low temperature embrittlement”, has been a matter of serious concern from the point of view of mechanical performance and lifetime of these alloys in the environment of fission as well as fusion reactors. It should be recognized that this concern about the loss of ductility due to neutron irradiation at relatively low temperatures (i.e. below the recovery stage V) is based exclusively on the results of post-irradiation mechanical tests.

In view of the fact that mechanical property changes are driven directly by microstructural changes, it is quite possible, however, that the mechanical response of structural materials in a fusion or fission reactor exposed simultaneously to an intense flux of energetic neutrons and external and internal stresses may be entirely different from those commonly observed during post-irradiation tests (see later for further discussion). In fact, the in-reactor tensile tests performed recently on pure copper and CuCrZr alloy [8] have demonstrated that indeed the deformation behaviour observed in the in-reactor tests is substantially different from that commonly observed in post-irradiation tests. However, since the damage accumulations during irradiation [9] as well as dynamic behaviour of dislocations are likely to be different in bcc iron and Fe-Cr alloy from that in fcc copper and copper alloys, it is important to investigate the in-reactor deformation behaviour of bcc iron and Fe-Cr alloy. The results of these investigations would be valuable not only from technological points of view but would also provide useful and realistic guidelines for understanding and modelling the deformation behaviour of bcc materials under the condition of dynamic deformation and damage production in reactor environment. With these considerations in mind, it was decided to determine experimentally the deformation behaviour of pure iron and Fe-Cr alloy during uniaxial tensile tests performed directly in a fission reactor (i.e. in the environment of fission neutrons). The present report describes the details of the tests and the main results on the mechanical response of the materials

during the tests. The results of post-irradiation and deformation microstructural investigations are also presented.

2 Materials and Experimental Procedure

2.1 Materials

Materials investigated in the present work were pure iron and Fe-9 % Cr alloy. Thin sheets (0.25 mm thick) of pure iron (see Table 1 for composition) were purchased from Good Fellow (England) in the cold-worked state. Tensile specimens (see Figure 1 for dimensions and geometry) were fabricated from these sheets and were given a heat treatment at 923 K for 2 h in vacuum ($\sim 10^{-6}$ Torr). This heat treatment gave an average grain size of $\sim 30 \mu\text{m}$ and a dislocation density of $\sim 10^{12} \text{ m}^{-2}$.

Table 1. Chemical composition (in wt%) of iron and Fe-Cr alloy

Alloy	C	Mn	Si	P	S	Cr	Ni	Mo	Cu	N	O
Fe	0.0090	0.0003	0.0015	0.0003	0.0002	0.0008	0.0002	0.0007	0.0004	-	-
FeCr	0.002	0.007	0.006	0.005	0.005	9.02	0.008	0.006	-	0.014	0.013

In order to avoid water corrosion of iron specimens during the in-reactor tensile tests, the tensile specimens were coated with a thin layer ($\sim 10 \text{ nm}$) of platinum. Coated specimens were examined in a scanning microscope to determine the quality of the coating. The surface topography of the coated specimens demonstrated that the quality of coating was perfectly acceptable (Figure 2 (a)). The coated specimens were then deformed in a tensile testing machine to a strain level of 20 %. The deformed specimens were examined again in a scanning microscope. The surface topography (Figure 2 (b)) of the coated specimens showed that the coated layer survived during the tensile test very well and would be expected to provide the necessary protection against water corrosion during the in-reactor tensile tests.

A small slab of pure and single phase Fe- 9 % Cr alloy (see Table 1 for composition) was obtained from Dr. P. Spaetig (EPFL/CRPP, Villigen-PSI, Switzerland). The as-supplied alloy had received a solution annealing heat treatment at 1223 K for one hour followed by annealing at 1073 K for 24 h and then furnace cooled. The final grain size of the alloy was about $105 \mu\text{m}$. A number of 0.5 mm thick tensile specimens were spark cut from the slab (see Figure 1 for dimensions and geometry). These tensile specimens were given no further heat treatment prior to irradiation and the in-reactor or out-of-reactor tensile testing.

2.2 Test module and irradiation rig

In order to carry out uniaxial tensile tests in the neutron environment of a fission reactor, a special test facility consisting of a pneumatic tensile test module and a servo-controlled pressure adjusting loop was designed and constructed. The pressure adjusting loop operates on a continuous flow of helium gas through an electrically controlled servo valve.

The basic principle of the tensile test module is based on the use of a pneumatic bellow to introduce stress and a Linear Variable Differential Transformer (LVDT) sensor to measure the resulting displacement produced in the tensile specimen. The movement of the bellows is controlled by LVDT sensor which also gives the feedback signal for the servo controller. Details of such a test facility have been described earlier [10] and therefore would not be repeated here. A number of such test modules were extensively tested outside of the reactor for their functional performance and reliability. The detailed design and geometry of the module was then adjusted to make it compatible with the irradiation conditions in the BR-2 reactor (i.e. the geometrical, neutronic, thermal and cooling environment).

To accommodate the test module and the necessary instrumentation to perform the uniaxial tensile test in the reactor, special irradiation rigs were designed and constructed at Mol. Figure 3(a) shows the simplified layout and operational features of the test module including the instrumentation. The photograph in figure 3(b) shows the final assembly of the test module, specimens and the necessary instrumentation. The whole assembly is loaded in the irradiation rig which is hung in a thimble tube. During the whole tensile test period, the irradiation rig remained submerged in the demineralised reactor pool water. To avoid overheating of the specimens due to gamma heating, the pool water was circulated in the irradiation rig at a rate of 600 liters of water per hour from the top of the test assembly. The temperature profile in each test module was measured by three thermocouples placed at three different positions (i.e. LVDT, specimen and the bellow) in the rig (see Figure 3(a)). Three dosimeters were placed at the specimen level to measure the neutron fluence.

2.3 In- reactor uniaxial tensile tests

The irradiation rig was designed to accommodate two complete test modules such that two independent tensile tests can be performed at the same time. In addition, a tensile specimen was attached to each test module which was irradiated in unstressed condition but with the same neutron flux and at the same temperature as for the in-reactor tensile test specimen. These specimens were used for the post-irradiation (out of reactor) tensile tests and microstructural investigations in the as-irradiated and post-irradiation deformed conditions.

In the first in-reactor deformation experiment, two test modules containing tensile specimens of Fe-Cr alloy were loaded in the irradiation rig.

The rig was manually inserted into the open thimble tube at position F46 of the BR-2 reactor core during the steady state operation of the reactor. As the rig was lowered in the open tube, the temperature of the test modules increased rapidly due to the gamma heating power of 2.5 Wg^{-1} and the circulating reactor pool water close to test specimens reached an equilibrium temperature of about 325K within a few minutes. Note that the test temperature of each test module and the specimen was measured and recorded separately. The test specimen was loaded when a stable temperature of 325 K was reached. Both the test specimen and the reference specimen attached to the test module received a neutron flux of $3.3 \times 10^{17} \text{ n/m}^2 \text{ s}$ ($E > 1 \text{ MeV}$) corresponding to a displacement damage rate of $4.7 \times 10^{-8} \text{ dpa}$ (displacement per atom)/s.

The first in-reactor uniaxial tensile test (henceforth referred to as Test No. 1) was started about 17 min. after the rig was inserted in the reactor core. In other words, the tensile specimen received a displacement dose of $4.8 \times 10^{-5} \text{ dpa}$ while it was still without any load (see Table 2). The tensile test was carried out at a constant strain rate of $1.0 \times 10^{-7} \text{ s}^{-1}$. This rather low strain rate was chosen to ensure that the specimen should survive the in-reactor deformation for long enough time to accumulate a displacement dose level of about 0.1 dpa. This was considered to be necessary to assess the dynamic effects of irradiation and the applied stress on the deformation behaviour of the specimen. During the test, the movement of the bellow (i.e. extension of the specimen) was measured continuously with the LVDT sensor and recorded continuously. To avoid fracture and separation of the specimen into two halves, the tensile test was terminated at $\sim 64 \%$ of the maximum load.

The second in-reactor tensile test on the Fe-Cr specimen in the second test module (henceforth referred to as Test No. 2) was started about 70.5 hours after the rig was inserted in the reactor core. Thus, the specimen accumulated displacement damage at the test temperature of 327 K to a dose level of $1.0 \times 10^{-2} \text{ dpa}$ without experiencing any applied stress (see Table 2). The test was carried out with a strain rate of $1.0 \times 10^{-7} \text{ s}^{-1}$ and a damage rate of $3.9 \times 10^{-8} \text{ dpa/s}$. The test was terminated at $\sim 78 \%$ of the maximum load to avoid the fracture and separation of the specimen into two halves.

The Test No. 3 was carried out some months later as a part of another series of experiments. However, the test modules and the irradiation rig were identical to the ones used for the Tests No. 1 and 2. In this test the platinum coated tensile specimen of pure and fully annealed (923 K/2 h) iron was loaded in the same manner as described before. The irradiation rig loaded with two test modules was inserted in the open thimble tube in position H 337 of the BR-2 reactor core during the steady state operation of the reactor. During this test, the test temperature equilibrated at 325 K and remained almost constant during the whole test period. The stress, strain and the test temperature were measured and recorded in the same manner as for the Tests No. 1 and 2. The test was carried out with a strain rate of $1.0 \times 10^{-7} \text{ s}^{-1}$ and at a displacement damage rate of $4.6 \times 10^{-8} \text{ dpa/s}$. The tensile test No 3 was started after the specimen had received a displacement dose of about $2.7 \times 10^{-4} \text{ dpa}$ (see Table 2). The test was terminated at $\sim 37 \%$ of the maximum load.

The second platinum coated tensile specimen of pure iron was loaded in the second test module in this series of experiments. The main objective of this

test, Test No. 4, was to determine the effects of pre-yield dose level on the deformation behaviour during the in-reactor tensile test, Therefore the specimen used in Test No 4 was irradiated at the test temperature of 323 K for about 70 h at a damage rate of 3.5×10^{-8} dpa/s giving a damage level of 8.9×10^{-3} dpa. In other words, the damage accumulation in the specimen used in the Test No 4 took place in the absence of applied stress for a period of ~ 70 h corresponding to a displacement dose level of 8.9×10^{-3} dpa.

Table 2 Displacement dose levels at various stages of in-reactor tensile tests

Material	Sample Number	Test Number	$T_{\text{irr}} = T_{\text{test}}$ (K)	Damage Rate (dpa/s)	Displacement Dose (NRT dpa) at			
					start of tensile test	yield point	end of tensile test	end of irradiation
Fe-Cr	FC-20	No 1	325	4.7×10^{-8}	4.8×10^{-5}	1.1×10^{-3}	5.7×10^{-2}	7.8×10^{-2}
Fe-Cr	FC-19	No 2	327	3.9×10^{-8}	1.0×10^{-2}	1.1×10^{-2}	6.5×10^{-2}	6.5×10^{-2}
Fe	FEN 12	No 3	325	4.6×10^{-8}	2.7×10^{-4}	5.7×10^{-4}	3.5×10^{-2}	3.6×10^{-2}
Fe	FEN 15	No 4*)	323	3.5×10^{-8}	8.9×10^{-3}	—	2.7×10^{-2}	2.7×10^{-2}

* Test not completed because of mechanical failure

2.4 Microstructural Investigations

The microstructure of samples in various states (e.g. unirradiated, unirradiated and deformed, as-irradiated, irradiated and deformed and in-reactor deformed) was investigated using a JEOL 2000FX transmission electron microscope (TEM). Thin foils for TEM examination were prepared by twin-jet electropolishing. Thin foil of Fe-Cr alloy were prepared by electropolishing in a solution of 20 % perchloric acid and 80 % ethanol at 12 V and at 253 K. Specimens of pure iron were electropolished at 18 V and at 253 K in slightly different solution containing only 10 % of perchloric acid and 90 % of ethanol. Prior to electropolishing, the TEM discs were mechanically polished down to a thickness of ~ 120 μm . For the investigation of the post-deformation microstructure, 1 mm wide strips were cut out of the gauge length of tensile specimens.

3 Differences between Post-irradiation and In-reactor Tensile Tests

Before presenting the results of the in-reactor tensile tests, it is of crucial importance to clarify the fundamental differences between the conventional post-irradiation tests and the in-reactor dynamic tensile tests so that the results of these two completely different types of tensile tests could be compared and contrasted properly. In addition, in order to get a proper insight into the deformation processes and to be able to appreciate the complications involved in the in-reactor dynamic tests, it is necessary to understand the details of the unique features of these tests. In the following, these features and their main implications are briefly described.

3.1 Post-irradiation Tensile Tests

In the case of traditional post-irradiation tensile tests, the specimens are first irradiated in unstressed condition to a certain displacement dose level at a certain irradiation temperature to accumulate displacement damage in the form of defects and their clusters. The irradiated specimens are then tensile tested outside of a reactor (i.e. in the absence of irradiation environment). During irradiation at relatively low temperatures (i.e. below the recovery stage V), the irradiation induced clusters appear in the form of loops and nanovoids (i.e. in bcc iron) and loops and SFTs (e.g. in fcc copper) with a homogeneous distribution throughout the whole crystal. In addition, the glissile SIA loops produced in the cascades both in fcc and bcc crystals are likely to segregate on grown-in dislocations forming a single or multi-layer cloud of loops along the dislocations. These glissile loops have also been observed to form rafts of small loops in bcc metals.

Thus, it is this microstructure containing SIA loops, nanovoids (or SFTs) and decorated dislocations (and/or rafts of SIA loops) present at the end of the irradiation that would respond to the applied stress during the post-irradiation tensile tests performed outside of a reactor. In other words, the mechanical response measured during these post-irradiation tests in terms of yield stress, post-yield flow stress, uniform and total elongations are entirely determined by the “frozen-in” microstructure. It is worth emphasizing here that since plastic deformation during post-irradiation tensile tests occurs in the absence of continuous generation and accumulation of defects and their clusters, the mechanical response measured during these tests do not provide any information about the dynamic effects of continuous production of defects and their clusters and their interaction with concurrently produced mobile dislocations by the applied stress.

It is well established that during irradiation (in the absence of applied stress) at temperatures below the recovery stage V, the damage accumulation occurs rather rapidly with increasing irradiation dose. Consequently, during post-irradiation tensile tests of specimens irradiated to dose levels beyond ~0.1 dpa (e.g. in copper) the initiation of plastic deformation (i.e. yielding) occurs at high stresses exhibiting yield drop, plastic flow localization (in the form of cleared channels) and almost a complete lack of work hardening. This makes it practically impossible to study the evolution of plastic flow (beyond yielding) and work hardening behaviour as a function of strain. From the practical application point of view, on the other hand, it is crucially important to know

the plastic flow and work hardening behaviour after yielding so that the lifetime of the material under applied stress could be assessed. Clearly, this kind of information cannot be obtained from the results of post-irradiation tests.

3.2 In-reactor Tensile Tests

In contrast to the post-irradiation tests, during in-reactor tensile tests the specimens are exposed simultaneously to applied stress (at a constant strain rate) and displacement damage produced by the flux of neutrons (at a constant damage rate). These conditions closely represent the conditions under which materials in the structural components of a fission or fusion reactor will have to deform and survive. During the present in-reactor tensile tests, the mechanical response of the specimen in terms of stress build up is continuously measured and recorded as a function of increasing strain (and displacement dose) in the form of a “dynamic” stress-strain curve representing the combined effect of the strain rate and the damage rate experienced by the specimen. Thus, the in-reactor tensile tests make it possible to determine the evolution of the flow stress as function of dose (and strain) even beyond the yield point. As mentioned in the previous section, this can not be achieved in the post-irradiation tests.

It should be recognized, however, that although the in-reactor dynamic tests are extremely interesting as well as realistically representative of in-reactor practical situation, the processes of damage accumulation, microstructural evolution and plastic deformation are thoroughly complicated. The complications arise primarily because of the involvement of simultaneously occurring two interactive kinetics in the evolution of the microstructure and the corresponding mechanical response at a given displacement dose level (or at a given time or strain rate). Furthermore, it is extremely difficult to determine experimentally the contributions of these two kinetics (one driven by the damage rate and the other driven by the strain rate) to the microstructural evolution and the corresponding mechanical response. The increase in the flow stress with increasing strain (and dose) measured in the present in-reactor tensile tests, for example, is a complicated combination of strain hardening due to increase in dislocation density and radiation hardening due to increase in the density of irradiation-induced defect clusters and the decoration of dislocation segments. A further complication during the in-reactor deformation experiments is likely to arise because of the existence of a population of mobile dislocations produced and driven by the applied stress. Under these conditions the mobile dislocations are likely to drag the loops decorating them. This may cause additional interaction between the loops in the decoration and the sessile loops, SFTs or nanovoids in the matrix. Consequences of these interactions and their impact on the stress response of the mobile dislocations will have to be estimated. Thus, the mechanical response of materials tested under these conditions would be expected to be significantly different from the response observed during post-irradiation tests. A great caution should be exercised, therefore, while comparing the results of the in-reactor tests and the post-irradiation tests.

4 Experimental Results

In the present section, the results will be presented in two blocks. We shall first describe the main results of mechanical testing carried out not only in the reactor but also tests performed out side of reactor (i.e. in the absence of neutron environment) on the unirradiated reference specimens as well as post-irradiation tests performed on specimens irradiated together with the in-reactor tests but in the unstressed condition. This will be followed by the description of the main results of microstructural investigations.

4.1 Mechanical response

As mentioned earlier, during the in-reactor tensile test, a specimen experiences simultaneously an externally applied stress (to maintain a constant strain rate) and a flux of defects and defect clusters produced by neutrons. It is of interest; therefore, to examine first of all the measured raw results on build up of stress and strain in the specimens as a function of irradiation (and tensile test) time and the displacement dose level. It should be noted that during the in-reactor tensile tests, the evolution of both stress and strain in the specimen is continuously measured and recorded.

The evolution of stress in the specimens of Fe-Cr alloy used in the Test No. 1 and Test No. 2 is shown in Figure 4(a) and Figure 4(b), respectively, as a function of irradiation (and tensile test) time and displacement dose. As can be seen in Figure 4, the actual tensile test on the specimens in the Test No. 1 (Figure 4(a)) and Test No. 2 (Figure 4(b)) were initiated at different times after the specimens were brought in the reactor. It can be also seen that the specimens in the Test No. 1 and Test No. 2 yielded at different stress levels (see Figures 4(a) and 4(b)) simply because they received different displacement doses before the tensile test was initiated (see Table 2). Doses at which the yield point was observed in the Test No. 1 and Test No. 2 and doses at which these tests were discontinued are also given in Table 2. The tensile properties of unirradiated, post-irradiated and in-reactor tensile tested specimens of Fe-Cr alloy are summarized in Table 3.

In order to make the results of the in-reactor tests comparable with the conventional tensile test results, we have transformed the raw results presented in Figure 4 into conventional stress-strain curves and the results are shown in Figure 5. This transformation is straightforward since these tests are performed at a constant strain rate which is continuously measured during each test. For comparison purposes, the stress-strain curves for the unirradiated Fe-Cr alloy are also shown in Figure 5. It should be noted that the unirradiated specimens were tested at room temperature (i.e. 293 K) and at higher strain rates.

Together with the specimens used in the in-reactor Test No. 1 and Test No. 2, two reference specimens of Fe-Cr alloy were irradiated in the unstressed condition and at the same irradiation temperature as specimens in the in-reactor

tests No. 1 and 2 and until the in-reactor tensile tests were terminated and the rig was taken out of the reactor. The dose accumulated in these reference specimens are quoted in Table 2. These irradiated specimens were tensile tested in a standard tensile testing machine at a strain rate of $1.3 \times 10^{-3} \text{ s}^{-1}$. Unfortunately these specimens got tested by mistake at 423 K. The stress-strain curves for the post-irradiation tested specimens are shown in Figure 6 and the numerical values for the mechanical properties are quoted in Table 3. The unirradiated specimens of Fe-Cr alloy were also tested with a strain rate of $1.3 \times 10^{-3} \text{ s}^{-1}$ at 333 K and the stress-strain curve is also shown in Figure 6.

Table 3 Tensile properties of unirradiated, post-irradiated and in-reactor tensile tested pure iron and Fe-Cr alloy

Material	Test condition	Test No.	T_{irr} (K)	T_{test} (K)	$\dot{\epsilon}$ (s^{-1})	σ_y (MPa)	$\sigma_{0.2}$ (MPa)	σ_{max} (MPa)	ϵ_u (%)	ϵ_t (%)
Fe-Cr	Unirradiated	1742	-	295	1.3×10^{-3}	120	155	321	15	17
„		1743	-	295	1.3×10^{-3}	130	160	322	14	17
„		1744	-	295	1.3×10^{-3}	130	163	323	15	19
Fe-Cr	Unirradiated	VTT	-	293	9×10^{-5}	158	168	315	19.5	(*)
Fe	Unirradiated	1745	-	295	1.3×10^{-3}	135	115	207	13	15
„		1746	-	295	1.3×10^{-3}	115	110	199	12	15
„		1747	-	295	1.3×10^{-3}	145	130	220	11	14
Fe	Unirradiated	VTT	-	293	1×10^{-7}	50	79	240	16.3	(*)
Fe-Cr	Post-irradiated	1769	327	423	1.3×10^{-3}	350	330	349	5	7
		1770	325	423	1.3×10^{-3}	340	325	344	5	7
Fe	Post-irradiated	1825	325	323	1.3×10^{-3}	180	183	190	0.2	3.2
Fe-Cr	In-reactor	Test No 1	325	325	1×10^{-7}	235	290	518	7.5	12.0*)
Fe-Cr	Tested	Test No 2	327	327	1×10^{-7}	390	395	538	10.7	14.3*)
Fe	„	Test No 3	325	325	1×10^{-7}	99	125	201	4.1	7.4*)

(*) Tensile test was interrupted

Traditionally, the magnitude of the effect of irradiation on hardening behaviour of metals and alloys is evaluated in terms of the dose dependence of the increase in the yield stress in the post-irradiation tensile tests. As indicated earlier, the dose dependence of the flow stress in the post-yield deformation regime cannot be determined from the post-irradiation tensile tests. The in-reactor tensile tests make it possible, on the other hand, to study the combined effect of irradiation dose and plastic strain on the evolution of flow stress as a function of strain (and dose) in the post-yield deformation regime.

The variation of the increase in the flow stress, $\Delta\sigma_f$, due to irradiation is shown in Figure 7 as a function of true strain during the in-reactor Test No. 1 and Test No. 2. The magnitude of $\Delta\sigma_f$ is obtained simply by subtracting the flow stress of the unirradiated specimen (Figure 5) from that of the flow stress of the in-reactor test (Figure 5) at a given strain (i.e. dose) level. It is interesting to note that the $\Delta\sigma_f$ increases faster with increasing true strain in the case of Test No. 1 than that in the Test No. 2. As a matter of fact, in the case of Test No. 2, $\Delta\sigma_f$ remains almost unchanged with increasing true strain. Furthermore, the $\Delta\sigma_f$ value saturates at somewhat higher level in the Test No. 1 than that in the Test No. 2.

Before presenting the results of the in-reactor tests on pure iron, it is useful to summarize the results on Fe-Cr alloy presented in Figures 4-7. The results illustrate the following interesting features:

- (i) The specimens of Fe-Cr alloy do not show occurrence of yield drop neither during the out-of-reactor tests in the unirradiated condition nor during the in-reactor tests (Figures 4 and 5). However, the phenomenon of yield drop is clearly observed during the post-irradiation test of Fe-Cr alloy irradiated to displacement doses of 7.8×10^{-2} dpa and 6.5×10^{-2} dpa (Figure 6).
- (ii) The yield stress increases with increasing pre-yield dose (Figure 5).
- (iii) The increase in the post-yield flow stress with increasing strain (dose) is faster in the specimen with lower pre-yield dose (i.e. Test No. 1) (Figure 5).
- (iv) The magnitude of the maximum flow stress is not affected by the pre-yield dose level (Figure 5).
- (v) The strain (dose) dependence of $\Delta\sigma_f$ is noticeably stronger in specimen with lower pre-yield dose (Test No. 1) than that in the specimen with higher pre-yield dose (Test No. 2) (Figure 7).
- (vi) The pre-yield dose does not seem to affect the uniform elongation during the in-reactor tensile tests (Figure 5) No. 1 and No. 2.

The engineering stress measured during the in-reactor Test No. 3 on pure iron carried out at 325 K is shown in Figure 8 as a function of irradiation and tensile tests time and displacement dose level. The true stress-true strain curve for the in-reactor Test No. 3 is plotted in Figure 9. The true stress-true strain curve for the unirradiated pure iron tested out side of reactor at 293 K is also shown in Figure 9. The out-of-reactor test on the unirradiated specimen was performed in a test module like the one used in the in-reactor test. It should be noted that the test was performed with a strain rate of $1 \times 10^{-7} \text{ s}^{-1}$. The test conditions are summarized in Table 2 and the mechanical properties for the in-reactor and out-of-reactor tensile tests are quoted in Table 3. It should be noted that just like Fe-Cr specimens, the specimens of pure iron do not exhibit the phenomenon of yield drop neither during the in-reactor test nor in the out-of-reactor test on the unirradiated specimens, with a strain rate of $1 \times 10^{-7} \text{ s}^{-1}$. It should be noted, however, that the specimen of the same pure iron tested at 295 K with a strain rate of $1.3 \times 10^{-3} \text{ s}^{-1}$ does exhibit a clear yield drop (see Figure 10). It is somewhat surprising that the magnitude of hardening during the in-

reactor tensile test (Test No. 3) on pure iron is rather low and at the same time the test yields rather low uniform elongation (see Table 3).

Figure 10 shows the stress-strain curve for the post-irradiation tensile test on pure iron irradiated to a dose level of 3.6×10^{-2} dpa at 325 K. The post-irradiation test was carried out in a standard tensile testing machine with a strain rate of $1.3 \times 10^{-3} \text{ s}^{-1}$. For comparison, the stress-strain curve for the unirradiated iron specimen tested at 293 K with a strain rate of $1.3 \times 10^{-3} \text{ s}^{-1}$ is also shown in Figure 10. Both the unirradiated and the post-irradiated specimens exhibit yield drop although the yield drop is sharper and deeper in the unirradiated specimen than that in the post-irradiated specimen. Furthermore, the post-irradiation test exhibits a significant reduction in the uniform elongation and the work hardening ability.

In order to illustrate the effect of irradiation on the hardening behaviour of pure iron during the in-reactor tensile test (No. 3) in the post-yield deformation regime, the change in the flow stress, $\Delta\sigma_f$, caused by irradiation is plotted in Figure 11 as a function of true strain. Note that the values of $\Delta\sigma_f$ are obtained from the results shown in Figure 9. It is interesting to note that even though the pre-yield dose in this test is rather low ($\sim 5.7 \times 10^{-4}$ dpa), still the increase in $\Delta\sigma_f$ reaches its maximum value at a very low strain (dose) and then does not change much with increasing strain (dose). This behaviour is clearly very different from what is observed in the case of Fe-Cr alloy (Test No. 1).

Figure 12 shows photographs of the in-reactor tested specimens of Fe-Cr alloy and pure iron after they were taken out of reactor and refer to the in-reactor tests (a) Test No. 1 (# FC 20), (b) Test No. 2 (#FC 19) on Fe-Cr alloy and (c) Test No. 3 (FEN 12) on pure iron. In order to avoid fracture of specimens into two halves, the in-reactor tests were interrupted by unloading the specimens during the rapid drop in the stress level while the specimens were necking. As can be seen in Figure 12, the specimens used in the Test No. 1, 2 and 3 did not break. The specimens used in the in-reactor Test No. 1, 2 and 3 yielded a total elongation of 12.0, 14.3 and 7.4 %, respectively (see Table 3).

4.2 Microstructural response

It is well known that the mechanical response of materials during deformation is determined by the details of the microstructure present at a given time (or strain) during the deformation. During in-reactor deformation, the evolution of microstructure is, as described in section 3.2, rather complicated because of continuous production of defect clusters and their interactions with continuously evolving dislocation microstructure. As a result, it is very difficult, if not impossible, at present to predict the evolution of microstructure under the conditions of in-reactor deformation. In order to understand the mechanical response of the specimens determined during the in-reactor tensile tests, it is, therefore, not only relevant but extremely important to establish the details of microstructural changes due to deformation and irradiation during in-reactor tensile tests. In the present work, various aspects of dislocation microstructure have been investigated in specimen tensile tested (a) out-of-reactor in the unirradiated condition, (b) in the reactor environment and (c) in the post-irradiation condition. In the following, the main results of

these investigations are summarized. The population of irradiation-induced defect clusters surviving at the end of the in-reactor tensile tests has been also investigated and the main findings are reported in this section.

4.2.1 Dislocation microstructure in unirradiated and tensile tested specimens

In order to facilitate a better understanding of the effect of concurrent irradiation and deformation on the evolution of dislocation microstructure during the in-reactor tensile tests, it was deemed useful to investigate the evolution of dislocation microstructure in specimens tensile tested out side of reactor in the unirradiated condition. With this objective in mind, a number of interrupted tensile tests were carried out to strain levels of 1.0, 5.0 and 10 or 15 %. This range of strain values was chosen so that the results of these investigations could be compared and contrasted with the results of the in-reactor tensile tests which yielded total elongations in the range of 7.4 % to 14.3 % (see Table 3). In these interrupted tests a specimen is deformed in a conventional tensile testing machine to a given strain level and then the test is stopped and the specimen is removed for microstructural investigations. The test is repeated on different specimens to different strain levels. Thus, the dislocation microstructure observed in a deformed specimen is representative of the microstructure present in that specimen at the strain level when the test on that specimen was discontinued. These tests were carried out at 333 K with a strain rate of $1.3 \times 10^{-3} \text{ s}^{-1}$ on specimens of Fe-Cr alloy and pure iron. In the following the results of post-deformation dislocation microstructure are briefly summarized.

Fe-Cr Alloy

The post-deformation dislocation microstructures of unirradiated Fe-Cr alloy for the strain levels of 1.0, 5.0 and 15 % are illustrated in Figures 13, 14 and 15, respectively. The dislocation microstructure at 1.0 % strain level is shown in Figure 13. The microstructure at this strain level is dominated by the presence of relatively loose dislocation cells surrounded by tangled dislocations (Figure 13(a)). It is worth noting the presence of a few black-dot types of defect clusters in Figure 13(a). The black-dot type of contrast may arise from the presence of small loops or may be the projection of dislocation ends emerging at specimen surfaces. These possibilities are being investigated and the results will be reported later. As can be seen in Figure 13 (b), already at this low strain level a few loose and relatively long dislocation walls are also formed. This tendency continues at the strain level of 5.0 % where the microstructure is dominated by dislocation cells and cell walls (Figure 14 (a)). At this strain level (i.e. 5 %) the cells are more clearly defined and the cell walls are more densely packed with dislocations. In some part of the specimen, however, a number of rather dense and long walls of dislocations are observed (Figure 14(b)). It can be seen in Figure 14(b) that the volumes between these walls contain loose dislocation cells and tangled dislocations.

The dislocation microstructure at the 15 % strain level is completely dominated by the presence of dense walls of dislocations (Figure 15(a)). These walls are formed at an angle of about 55 degrees to the tensile axis. The trace

analysis suggests that these dense dislocation walls do not match any of the four {110} planes with the high Schmid factors. Traces of the {110} slip planes and the direction of the tensile axis is marked on Figure 15(a). It is interesting to note that the volumes between these dense dislocation walls are full of dislocation cells with relatively densely packed dislocation walls (Figure 15(b)).

Pure Iron

A number of specimens of pure annealed (at 923 K for 2 h) iron were tensile tested at 333 K with a strain rate of $1.3 \times 10^{-3} \text{ s}^{-1}$ in the unirradiated condition. The tests were interrupted at strain levels of 1.0, 5.0 and 10 %. The dislocation microstructures observed in the specimen deformed to 1.0 % plastic strain is shown in Figure 16. It can be seen that there is no clear indication of dislocation cell and cell wall formation. Dislocation population has fairly homogeneous distribution. However, in some areas a few dislocation tangles can be seen. It is interesting to note that, no dense and long walls of dislocations were observed in this specimen.

A very striking feature of the microstructure shown in Figure 16 is the presence a relatively high density of black-dot type of defect clusters. Some of these clusters have appearance of loops. However, at present the nature of these clusters remains unidentified. Appropriate investigations are in progress to characterize these clusters and the results will be reported later.

Figure 17(a) shows the microstructure of the specimen deformed to 5.0 % plastic strain. It can be seen in Figure 17(a) that the microstructure is completely dominated by the presence of dense dislocation walls. It is interesting to note that these walls separate regions with alternating light (A) and dark (B) contrast (Figure 17(a)), indicating an alternating change in the misorientation between the regions. The specimen showed also the formation of two sets of dense dislocation walls (see Figure 17(b)). The presence of loose dislocations and dislocation cells can be easily seen in Figure 17(a) as well as in Figure 17(b).

The dislocation microstructure in the specimen deformed to 10 % plastic strain (Figure 18) is rather similar to the microstructure observed in the specimen deformed to 5.0 % plastic strain. Figure 18 shows the presence of dense dislocation walls (parallel to $(\bar{1}10)$ trace) and loose dislocations and cells in the volumes between the dense dislocation walls.

4.2.2 Microstructure in the in-reactor tensile tested specimens

Fe-Cr Alloy, In-reactor Test No. 1

To investigate the microstructure induced by concurrent irradiation and deformation of specimens used in the in-reactor Test No. 1, thin foils for TEM examinations were prepared from the material taken from the middle of the gauge section of the tensile specimen used in the Test No. 1 (see Figure 12(a)). It is important to note that in the case of the in-reactor Test No. 1, the tensile test was started at a very low dose of 4.8×10^{-5} dpa (Table 2). When the Test No. 1 was interrupted, the specimen had reached a plastic strain of 12.0 % (see

Table 3), and a displacement dose of 7.8×10^{-2} dpa (Table 2). Figure 19 shows an example of the typical dislocation microstructure surviving at the end of the Test No. 1. The $\{011\}$ plane traces are marked by the dotted lines in Figure 19. The dislocation microstructure shown in Figure 19 mainly consists of homogeneously distributed three sets of almost straight dislocations. It is interesting to note that the straight dislocations are parallel to the traces of the three $\{011\}$ planes lying in the $[111]$ zone axis. Surprisingly, no segregation of dislocations in the form of dislocation cells and cell walls were observed in this specimen. It is worth mentioning here that this is significantly different result from the dislocation microstructure observed in the specimens deformed in the unirradiated condition (e. g. Figures 13, 14 and 15).

Figure 20 shows the weak beam dark field image illustrating the presence of very small defect clusters/loops in the specimen used in the in-reactor tensile Test No. 1. It should be pointed out that the weak beam image (Figure 20) was obtained from the same thin foil used for obtaining the dislocation microstructure shown in Figure 19. It can be seen in Figure 20(a) that inspite of 12.0 % of plastic deformation, a high density of very small clusters/loops survive in the specimen. It should be noted that these clusters/loops are homogeneously distributed. Figure 20(b) shows an example of areas containing small clusters/loops and a few straight dislocation lines. Judging from the contrast it seems as if the dislocation lines are decorated with the interstitial clusters/loops or clusters of Cr and self-interstitial atoms. However, the distribution of small clusters between the dislocation segments remains fairly homogeneous.

Fe-Cr Alloy, In-reactor Test No. 2

First of all it should be mentioned that the tensile test in the case of the in-reactor Test No. 2 was deliberately started at a relatively high dose level of 1.0×10^{-2} dpa (see Table 2). In other words, the specimen in this test received a displacement dose of 1.0×10^{-2} dpa in the absence of deformation induced mobile dislocations. This means that the grown-in dislocations present in the specimen at the time of the start of irradiation had plenty of time for the evolution of decoration at and around them. Just like in the case of Test No. 1, thin foils for the TEM examinations were prepared from the material taken from the middle of the gauge section of the tensile specimen used in the in-reactor Test No. 2 (see Figure 12(b)). When the Test No. 2 was interrupted, the specimen had reached a plastic strain of 14.3 % and a displacement dose of 6.5×10^{-2} dpa (see Table 2).

Examples of dislocation microstructure surviving at the end of the in-reactor Test No. 2 are shown in Figures 21(a), 21(b) and 21(c). The deformation microstructure in this specimen is dominated by extended and dense dislocation walls with loose and tangles of dislocations between the walls. Figure 21(a) shows an example of the presence of a set of almost parallel and long dislocation walls extending all the way to a grain boundary. As can be seen in Figure 21(a), the walls are approximately parallel to the trace of $(0\bar{1}1)$ plane. The edge-on (sharp) image of the walls and sample tilting experiments in TEM demonstrated that these dense dislocation walls are almost aligned with the $(0\bar{1}1)$ slip plane. Figure 21(b) shows high magnification view of two

adjacent extended dense dislocation walls and dislocation tangles and loose dislocations in the volume between the walls. Finally, Figure 21(c) shows an example of relatively loose dislocation walls and loose as well as tangled dislocations between the walls.

Figure 22(a) shows a weak beam dark field image of defect clusters in the specimen used in the in-reactor Test No. 2 and illustrates that the defects clusters/loops are fairly homogeneously distributed in the regions away from the dense dislocation walls. Since the dislocation microstructure in this specimen is dominated by loose and dense dislocation walls and tangled dislocations, (see Figure 21(b) and 21(c)), it is of interest to examine the influence of these dislocation walls and tangles on the overall cluster density and their spatial distribution. In general, the presence of dislocation walls appears to induce heterogeneity in the spatial distribution of the small clusters/loops. Figure 22(b) shows a weak beam dark field image of two dislocation walls (marked A and B) and defect clusters. Both dislocation walls are loose enough so that individual dislocations in the walls can be clearly imaged. As can be seen in Figure 22(b), practically all dislocations in the wall marked A are decorated with defect clusters and only a few clusters are visible in the volume between the dislocations. An enlarged version of the dislocation wall marked B in Figure 22(b) is shown in Figure 22(c) which shows the same features as seen in the Figure 22(b). Furthermore, the cluster density in the volume between the two dislocation walls also appears to be rather low.

In order to evaluate the accumulation of defect clusters/loops in the irradiated but undeformed part of the Fe-Cr specimen, thin foils were prepared from the material taken from the end of the “head” of the tensile specimen used in the in-reactor Test No. 2 (see Figure 12(b)), specimen marked FC 19). Since the “head” of the specimen is more than 3 times wider than the gauge width (see Figures 1 and 12(b)), the stress acting on this part of the specimen during the in-reactor Test No. 2 would be considerably below even the yield stress of the material. Therefore, no dislocations are expected to be generated in this part of the specimen during the in-reactor Test No. 2. TEM examinations of the thin foils taken from this part of the specimen showed no evidence of deformation induced dislocations. The displacement damage and irradiation temperature in this part of the specimen, on the other hand, are expected to remain the same as in the gauge section of the tensile specimen. Hence, the microstructure observed in this thin foil can be taken to represent the accumulation of defect clusters/loops in the absence of deformation induced mobile dislocation.

Figure 23 shows the weak beam dark field image of defect clusters in the thin foil taken from the undeformed region of the specimen tensile tested in the in-reactor Test No. 2 at 327 K to a displacement dose level of 6.5×10^{-2} dpa. A high density of homogeneously distributed small defect clusters/loops can be seen in Figure 23. The cluster size and density do not appear to be significantly different from the size and density of clusters shown in Figure 22(a) from the gauge section of the specimen tested in the in-reactor Test No. 2.

Pure Iron, In-reactor Test No. 3

Just like in the case of the in-reactor tested Fe-Cr alloy in the Test No. 1 and 2, TEM examinations were carried out on thin foils prepared from the

material taken from the middle of the gauge section of the specimen of pure iron used in the in-reactor Test No. 3. It is important to note that the in-reactor test was started at a dose level of 2.7×10^{-4} dpa and the test was interrupted at a dose level of 3.5×10^{-2} dpa (see Table 2). At the time when the Test No. 3 was interrupted, the specimen had reached a total strain of 7.4 % (Table 3) and a displacement dose of 3.5×10^{-2} dpa (see Table 2).

Figure 24(a) illustrates dislocation microstructure observed within a grain in the pure iron specimen tested in the in-reactor Test No. 3. As can be seen in Figure 24(a), the dislocation microstructure is dominated by two sets of rather straight dislocations parallel to the traces of $(\bar{1}01)$ and $(\bar{1}10)$ planes. In Figure 24(a), a third set of dislocations parallel to the trace of $(0\bar{1}1)$ plane can be also seen in the loose dislocation wall at the right hand side lower corner of the Figure 24(a). The formation of a microband parallel to the trace of $(\bar{1}10)$ plane is shown in Figure 24(b). Figure 23(c) shows the initial stage of the formation of a weak microband parallel to the trace of $(\bar{1}10)$ plane (indicated by arrows).

In an effort to investigate the microstructure in the irradiated but undeformed part of the iron specimen, thin foils were prepared from the material taken from the end of the “head” of the tensile specimen used in the in-reactor Test No. 3 (see Figure 12(c)). It should be noted that at the end of the Test No. 3 this specimen had received a total displacement dose of 3.6×10^{-2} dpa (see Table 2). The weak beam imaging showed the presence of very low density of defect clusters/loops. Because of the low density, so far it has not been possible to determine a reliable value of the defect cluster density. Effort is still being made to quantify the cluster microstructure and the results will be reported later.

It is worth mentioning here that this thin foil demonstrated the presence of a low density ($\sim 1 \times 10^{19} \text{ m}^{-3}$) of relatively large voids (~ 89 nm in diameter). The voids were found to be present throughout the whole thin foil. An example of voids is shown in Figure 25. Similar observations have been reported earlier for pure iron neutron irradiated at 333 K to a dose level of 0.1 dpa [11]. It should be noted however that in this case the iron specimen was helium implanted (with 100 appm at 323 K) prior to neutron irradiation.

4.2.3 Microstructure of post-irradiation tensile tested specimens

Fe-Cr Alloy

Thin foils for TEM investigations were prepared from the material taken from the middle of the gauge section of the Fe-Cr specimen tensile tested at 423 K in the post-irradiation condition. The tensile specimen was irradiated at 327 K to a dose level of 7.8×10^{-2} dpa and during out of reactor test yielded a total strain of 7.0 % (see Table 3). It should be noted that by mistake the post-irradiation test got performed at 423 K. Figure 26(a) shows a low magnification bright field image illustrating an overall microstructure of the post-irradiation tested specimen. A number of microbands extending over long distances ($> 10 \mu\text{m}$) can be seen in Figure 26(a). The higher magnification image of the microbands presented in Figure 26(b) shows the formation of dense

extended dislocation walls containing high dislocation density. It should be noted that the dislocation walls in this case (Figure 26(b)) are parallel to the $(\bar{1}01)$ trace. The misorientation angle across one of the well-developed walls was found to be 2.4 degree (Figure 26(b)). The matrix between the walls is full of straight dislocation lines which are aligned in the $\{110\}$ planes.

Pure Iron

Figure 27 shows the dislocation microstructure of pure iron after tensile testing at 323 K with a strain rate of $1.3 \times 10^{-3} \text{ s}^{-1}$ in the post-irradiation condition. The specimen was irradiated at 325 K (in the unstressed condition) to a dose level of $3.6 \times 10^{-2} \text{ dpa}$ (see Table 2). The post-irradiation tensile test yielded a total elongation of only 3.2 % (see Table 3). Traces of three $\{110\}$ planes and the tensile axis are marked on Figure 27. The main feature of the dislocation microstructure shown in Figure 27(a) is the homogeneous distribution of mainly isolated dislocation segments and the formation of dislocation walls. A number of dislocation walls extending up to a grain boundary can be seen in Figure 27(a). Three sets of dislocations parallel to three $\{110\}$ planes can be identified in Figure 26(a). The dislocation walls seen in Figure 27(a) are parallel to the $(0\bar{1}1)$ plane. Figure 27(b) shows the evidence for the formation of three sets of dislocation walls and these walls are aligned with the three $\{110\}$ planes. Furthermore, three sets of homogeneously distributed isolated dislocations can also be identified in Figure 27(b). These dislocations are also parallel to the traces of the three $\{110\}$ planes.

It is interesting to note here that according to Schmid factor calculation, among the three slip planes marked on Figure 27, the $(\bar{1}01)$ and $(0\bar{1}1)$ planes are found to have the highest Schmid factor values, indicating that these planes are the active slip planes. The value of Schmid factor for the $(\bar{1}10)$ plane, on the other hand, is found to be almost zero. It is not at all clear at present as to why and how the slip systems in the $(\bar{1}10)$ plane gets activated.

5 Discussion

As regards the mechanical response during the in-reactor tensile tests, first of all, it should be noted that the phenomenon of yield drop commonly observed in post-irradiation tests was not observed during the in-reactor tests on the specimens of Fe-Cr alloy and pure iron. This is consistent with the results obtained during in-reactor tensile tests on pure copper and CrCrZr alloy [8, 11]. However, the phenomenon of yield drop is clearly observed during the post-irradiation tests of Fe-Cr and pure iron specimens used in the present work (see Figures 6 and 10, respectively).

Our earlier results on the in-reactor irradiated pure copper [8] had demonstrated that both the yield stress and the post-yield flow stress were sensitively dependent on the level of the pre-yield dose (i.e. the displacement dose received by a specimen in the absence of deformation-induced mobile dislocations after yielding). In order to investigate the effect of pre-yield dose further in the case of bcc crystals, Fe-Cr specimens were tested at two different values of pre-yield dose (Figures 4 and 5). Unfortunately, in the case of pure iron, the experiment at the higher pre-yield dose had to be abandoned because of mechanical failure during this test. Thus the effect of pre-yield dose on the yield stress and the post-yield flow stress of pure iron remains unknown at present.

In the case of Fe-Cr alloy, the yield stress increases with increasing pre-yield dose (Figure 5). The increase in the post-yield flow stress, σ_f , with increasing strain (dose) is faster in the specimen with lower pre-yield dose (i.e. Test No. 1, Figure 5). Furthermore, the strain (dose) dependence of $\Delta\sigma_f$ (which is the effect of irradiation on the flow stress) is also noticeably stronger in the specimen with lower pre-yield dose (Test No. 1) than that in the specimen with higher pre-yield dose (Test No. 2, Figure 7). It should be pointed out that these effects are qualitatively very similar to what has been reported earlier for the in-reactor tensile tested pure copper [8].

It is rather interesting to note in Figure 5 that the magnitude of the pre-yield dose does not affect the level of the maximum post-yield flow stress in Fe-Cr alloy. This is just opposite to what was observed in the case of pure copper where the maximum flow stress was found to be strongly dependent on the magnitude of pre-yield dose [8]. Furthermore, unlike in the case of pure copper, the pre-yield dose does not have any effect on the uniform elongation of Fe-Cr alloy during in-reactor deformation (Figure 5, Table 3). The variation of irradiation induced increase in the flow stress, $\Delta\sigma_f$, with strain (dose) (see Figure 7) clearly shows that the irradiation makes very small contribution to the post-yield flow stress in the specimen with a pre-yield dose of 1.0×10^{-2} dpa. The results on the specimen with a pre-yield dose of 1.1×10^{-3} dpa illustrate, on the other hand, that the irradiation causes significant contribution to the increase in the post-yield flow stress, in a manner very similar to that observed

in the case of pure copper for a very similar level of pre-yield dose (i.e. 2.2×10^{-3} dpa, see Table 1 and Figure 8, in Ref. [8]).

The results on the mechanical performance of the in-reactor tensile tested pure iron specimen (Test No. 3, Table 2), presented in Figures 8, 9 and 11, are substantially different from that observed in the case of Fe-Cr alloy. For instance, in the post-yield plastic flow regime, the hardening rate (σ_f vs. ϵ) in pure iron with the pre-yield dose of 2.7×10^{-4} dpa (Table 2) is much lower than that in Fe-Cr alloy with a pre-yield dose of 1.1×10^{-3} dpa. Furthermore, both the level of hardening and the level of $\Delta\sigma_f$ saturate at a considerably lower strain (dose) value in pure iron than that in the case of Fe-Cr alloy. It is somewhat surprising that both the uniform elongation and total elongation are much lower in the case of pure iron even when the level of maximum hardening is much lower in pure iron than that in Fe-Cr alloy.

One of the striking features of the microstructural evolution during the in-reactor tensile deformation is the lack of cleared channel formation both in Fe-Cr alloy and pure iron. The post-irradiation tensile tested specimens of Fe-Cr and pure iron do exhibit the phenomenon of yield drop yet no cleared channels could be found in these specimens. An equally interesting feature exhibited by the in-reactor deformed Fe-Cr specimen (particularly with the low pre-yield dose of 1.1×10^{-3} dpa; Test No. 1) is that the deformation during this in-reactor test occurs in a completely homogeneous manner without any indication of flow localization. A typical micrograph presented in Figure 19 shows a relatively low density of almost uniformly distributed straight dislocation lines parallel to the traces of three $\{011\}$ planes lying in the $[111]$ zone axis. There is no indication of dislocation segregation in the form of cells and dislocation walls. It should be noted that the microstructure shown in Figure 19 represents the dislocation microstructure in Fe-Cr specimen deformed to a total strain level of 12.0 % (see Table 3). Clearly, the microstructure shown in Figure 19 is entirely different from the microstructure of Fe-Cr specimens deformed to 5% and 15 % (Figures 14 and 15) in the unirradiated condition. In the unirradiated Fe-Cr alloy, deformation induced dislocations begin to form dislocation walls already at a deformation level of 1.0 % (Figure 13(b)).

The dislocation microstructure (see Figure 24(a)) in the in-reactor deformed specimen of pure iron (Test No. 3) is very similar to that observed in the case of Fe-Cr specimen. Just like in the case of Fe-Cr specimen, the deformation microstructure in the in-reactor deformed pure iron specimen is entirely different from that in specimens deformed in the unirradiated condition to strain levels of 5 and 10 % (Figures 17 and 18, respectively). It should be noted here that the in-reactor deformed specimen in Test No. 3 yielded a total elongation of 7.4 % (see Table 3). However, in the case of pure iron, some dislocation segregation is found to occur in the form of loose dislocation walls (e.g. Figure 24(a)) and a few microbands (e.g. Figure 24(b)). Nonetheless, the microstructure shown in Figure 24(a) is dominated by two sets of dislocations parallel to $(\bar{1}01)$ and $(\bar{1}10)$ planes.

A comparison of dislocation microstructures observed in the Fe-Cr specimen tested in the in-reactor Test No. 1 (Figure 19) (with a pre-yield dose of 1.1×10^{-3} dpa) with that of the microstructures in the specimen tested in the

in-reactor Test No. 2 (with a pre-yield dose of 1.1×10^{-2} dpa) (Figure 21) clearly demonstrates that the level of the pre-yield dose has a significant influence on the evolution of dislocation microstructure during the in-reactor tests. In view of the fact that the level of pre-yield dose does not seem to affect the post-yield flow stress (beyond about 5 % plastic strain) (see Figure 5) in any significant manner, it is very difficult to comprehend as to what role the observed differences in the microstructure play in the evolution of the observed mechanical response.

The results presented in the previous section suggest that the evolution of dislocation microstructure during the in-reactor tests as well as post-irradiation tests is affected by the damage produced during neutron irradiation. During the in-reactor as well as post-irradiation tests, for example, the accumulation of dislocations produced by deformation appears to get reduced and no dislocation cells are formed. Furthermore, the slip systems even in the planes with Schmid factor value of almost zero are activated both in pure iron and Fe-Cr alloy during the in-reactor test as well as during the post-irradiation tests. Normally, in the unirradiated and deformed bcc crystals only two sets of dislocation walls are formed near the two highly stressed shear planes. Irradiation, on the other hand, causes the formation of three sets of dislocations and dislocation walls (both in the in-reactor and post-irradiation tests), one of which is almost perpendicular to the applied stress axis.

It is important to point out that during neutron irradiation of pure iron at 325 K (Test No. 3) a high density of nanovoids are likely to be formed already at the pre-yield dose of 5.7×10^{-4} dpa. Positron annihilation spectroscopy experiments have demonstrated, for example, that the neutron irradiation at ~ 343 K produces a high density ($\sim 2 \times 10^{23} \text{ m}^{-3}$) of “nanovoids” in pure iron already at a displacement dose level of 10^{-4} dpa [13, 14]. These nanovoids do not become visible in the TEM until a dose level of about 0.7 dpa is reached [14]. This implies that although the present TEM investigations on the iron specimen used in the Test No. 3 do not show the presence of nanovoids, a high density of nanovoids are likely to be present already at the pre-yield dose of 5.7×10^{-4} dpa (Test No. 3, Table 2). This means that the interactions between the deformation induced mobile dislocations and the nanovoids produced during the in-reactor tensile test are unavoidable. Therefore, in order to explain the evolution of the microstructure containing defect cluster/loops, dislocations and nanovoids and the mechanical response during the in-reactor tensile test, the consequences of interactions between the mobile dislocations and various components of the microstructure will have to be considered carefully.

It is relevant to point out that the possibility of the formation of nanovoids in Fe-Cr alloy during the in-reactor deformation experiment must be investigated because the presence of these nanovoids is likely to affect the movement and accumulation of dislocations.

6 Summary and Conclusions

First of all, it must be mentioned that the present work is a follow-up of our earlier investigations of the in-reactor tensile deformation behaviour of pure copper and a precipitation hardened CuCrZr alloy [8, 11]. The results described and discussed in the present report demonstrate that this kind of in-reactor deformation experiments although quite difficult and time consuming but can be performed successfully. Furthermore, the results of these in-reactor tensile tests have provided new, useful and interesting insight into the complicated nature of deformation processes that are likely to operate during the deformation of materials in the structural components of a fission or fusion reactor.

Both Fe-Cr alloy and pure iron deform in a homogeneous manner during the in-reactor tensile tests yielding uniform elongations of ~7.5 and 10.5 % in the case of Fe-Cr alloy and 4.1 % in the case of pure iron. The low uniform elongation of only 4.1 % in pure iron is somewhat surprising since the increase in the post-yield flow stress with strain (dose) in pure iron is rather low. The reason for this difference in the hardening behavior between Fe-Cr alloy and pure iron is not at all clear at present.

In the case of Fe-Cr alloy, an increase in the pre-yield dose led to an increase in the yield stress which is consistent with the effect of pre-yield dose on the yield stress of pure copper during in-reactor deformation. Note that the rate of increase in the flow stress is higher in the case of low pre-yield dose than that in the case of high pre-yield dose. This behaviour is also consistent with the results in the case of pure copper. It is important to note, however, that the level of the maximum post-yield flow stress is practically unaffected by the increase in the pre-yield dose in the case of Fe-Cr alloy. This is very different from the behaviour observed in the case of pure copper where the maximum flow stress is strongly affected by the pre-yield dose. Furthermore, the uniform and the total elongations are higher in the Fe-Cr specimen with a higher pre-yield dose. In the case of copper, on the other hand, both uniform and total elongations were found to decrease with increasing pre-yield dose.

The irradiation induced increase in the flow stress, $\Delta\sigma_f$, with strain (dose) is substantially reduced in the case of Fe-Cr specimen with the pre-yield dose level of 1×10^{-2} dpa.

It is rather significant that neither the in-reactor deformed nor the post-irradiation deformed specimens of Fe-Cr and pure iron show any evidence of cleared channel formation. This is entirely different from the observations reported for pure copper where cleared channel formation was observed both in the in-reactor deformed specimens and post-irradiation tested specimens. It should be noted, however, that the in-reactor deformed specimen of copper with a very low pre-yield dose of 7.5×10^{-4} dpa (Table 1 in [8]) did not provide any clear evidence for the formation of well developed clear channels even after 14 % of uniform plastic strain (Table 2 in [8]).

During the in-reactor deformation of Fe-Cr and pure iron specimens with low pre-yield dose of 1.1×10^{-3} dpa and 5.7×10^{-4} dpa, respectively, no segregation of dislocations in the form of dislocation cells was observed. Instead, rather straight segments of dislocations accumulated homogeneously and only to a modest density. In the case of pure iron, however, some loose dislocation walls were observed. Even post-irradiation deformation does not lead to the formation of dislocation cells neither in the Fe-Cr nor in the pure iron specimens.

The in-reactor tested specimen of Fe-Cr alloy to a higher pre-yield dose of 1.1×10^{-2} dpa, on the other hand, showed the formation of dense dislocation walls extending up to grain boundaries. The volume between these walls contains dislocation tangles and loose dislocations.

Post-irradiation tensile tested specimens of Fe-Cr alloy and pure iron showed the formation of dislocation walls. The volume between the walls was found to contain homogeneously distributed dislocation lines parallel to $\{110\}$ planes. In the post-irradiation deformed pure iron, three sets of dislocation walls were found to be aligned with the three $\{110\}$ planes.

Both in Fe-Cr alloy and pure iron, the slip systems in the planes with the Schmid factor value of almost zero were found to be activated during the in-reactor as well as the post-irradiation tensile tests. It should be pointed out that this must be a specific effect of irradiation since normally in the unirradiated and deformed bcc crystals only two sets of dislocation walls are formed near the two highly stressed shear planes (i.e. with the top values of Schmid factor).

The results presented and discussed in the earlier sections on the mechanical and microstructural features determined in the in-reactor deformed specimens of Fe-Cr and pure iron clearly show that a number of interesting and important features of the results can not be rationalized properly because of the lack of experimental facts and guidelines. The most serious problem arises because of the lack of knowledge about the evolution of the defect clusters and dislocation microstructure as a function of plastic strain and displacement dose during the in-reactor deformation experiments. At present, we know only the final microstructure present at the end of the in-reactor deformation experiments. It would be, therefore, of a great help to obtain the experimental results on mechanical response and the corresponding microstructure at different levels of plastic strain (displacement dose). This kind of information can be readily obtained by carrying out a series of in-reactor interrupted tensile tests.

Acknowledgements

The present work was partly funded by the European Fusion Technology Programme. The authors would like to thank a number of technical staff members at VTT, Mol and RISØ for their valuable help in carrying out the present experiments. The authors are very grateful to Dr. P. Spaetig (EPFL/CRPP, Villigen PSI, Switzerland) for providing us the Fe-Cr alloy used in the present investigations.

References

- [1] R. L. Klueh, K. Ehrlich and F. Abe, J. Nucl. Mater. 191-194 (1992) 116.
- [2] L. K. Mansur, A. F. Rowcliffe, R. K. Nanstad, S. J. Zinkle, W. R. Corwin and R. E. Stoller, J. Nucl. Mater. 329-333 (2004) 166.
- [3] K. Ehrlich and K. Anderko, J. Nucl. Mater. 171 (1990) 139.
- [4] R. L. Klueh and D. R. Harries, High-Chromium Ferritic and Martensitic Steels for Nuclear Applications, American Society for Testing and Materials, West Conshohocken, PA, 2001.
- [5] D. S. Gelles, J. Nucl. Mater. 212-215 (1994) 714, J. Nucl. Mater 233-237 (1996) 293.
- [6] J. M. Vitek, W. R. Corwin, R. L. Klueh and J. R. Howthorne, J. Nucl. Mater. 141-143 (1986) 948.
- [7] V. S. Khabarov, A. M. Dvoriashin and S. I. Porollo, J. Nucl. Mater. 233-237 (1996) 236.
- [8] B. N. Singh, D. J. Edwards, S. Tähtinen, P. Moilanen, P. Jacquet and J. Dekeyser, Risø Report No. Risø-R-1481 (EN), October (2004), 47 p.
- [9] B. N. Singh, and J. H. Evans, J. Nucl. Mater. 226 (1995) 277.
- [10] P. Moilanen, S. Tähtinen, B. N. Singh and P. Jacquet, VTT Research Report BTU076-031127, VTT Technical Research Centre of Finland, Espoo, Finland, (2004), 24 p.
- [11] B. N. Singh, M. Eldrup, S. I. Golubov, D. J. Edwards and P. Jung, Risø report No. Risø-R-1496(EN), January (2005), 38 p.
- [12] B. N. Singh, S. Tähtinen, P. Moilanen, P. Jacquet and J. Dekeyser, J. Nucl. Mater, 320 (2003) 299.
- [13] M. Eldrup, B. N. Singh, S. J. Zinkle, T. S. Byun and K. Farnell, J. Nucl. Mater. 307-311 (2002) 912.
- [14] S. J. Zinkle and B. N. Singh, J. Nucl. Mater. 351 (2006) 269.

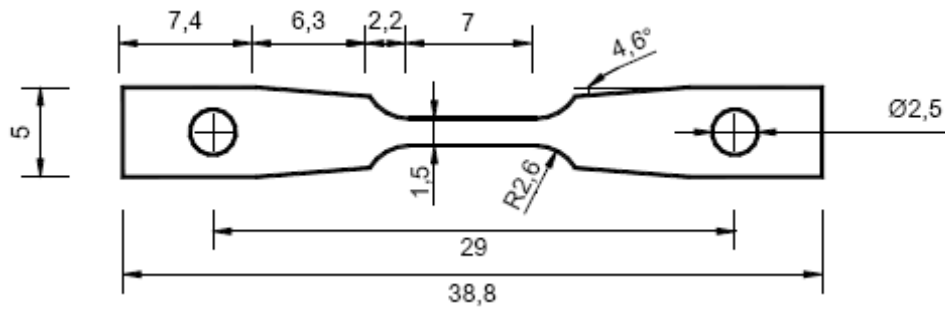


Figure 1. Size and geometry of tensile specimens used in the present investigations.

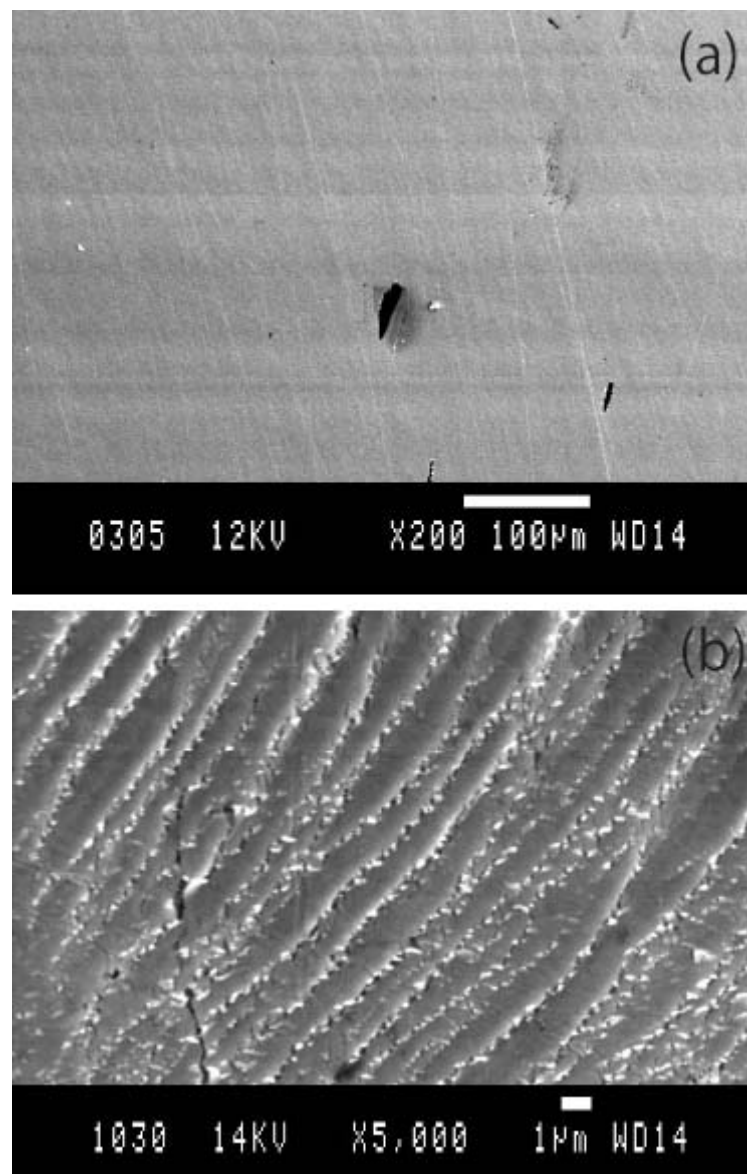


Figure 2. Surface topography of iron specimen coated with a thin (~10 nm) layer of platinum in (a) as-coated and (b) deformed (to 20 % strain after coating) conditions.

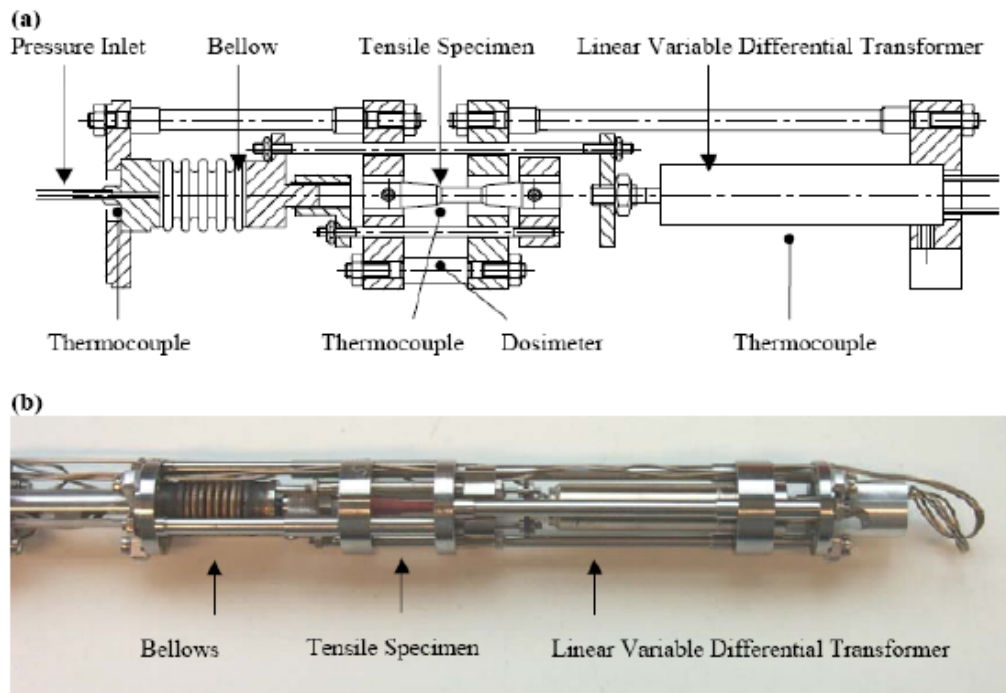


Figure 3. (a) Simplified layout and operational features of the test module used in the in-reactor tensile tests and (b) a photograph of the final assembly of the complete test module in the instrumented irradiation rig.

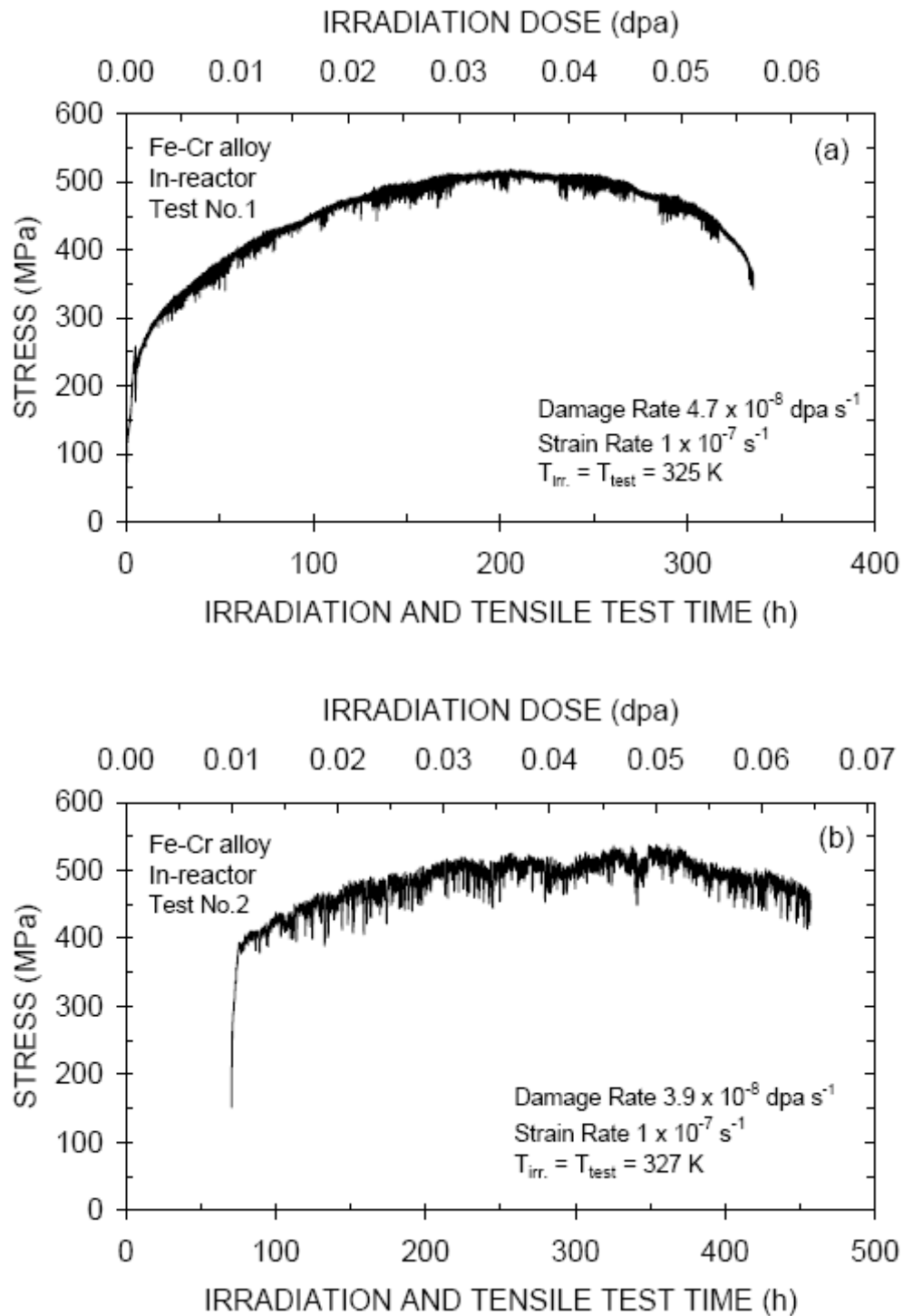


Figure 4. Continuously measured stress response of the Fe-Cr specimens as a function of irradiation and tensile test time (i.e. displacement dose) during the in-reactor tests (a) Test No. 1 with a pre-loading dose of $4.8 \times 10^{-5} \text{ dpa}$ and (b) Test No. 2 with a pre-loading dose of $1.0 \times 10^{-2} \text{ dpa}$. The pre-loading dose refers to the displacement dose that the specimen received before the actual tensile test was activated.

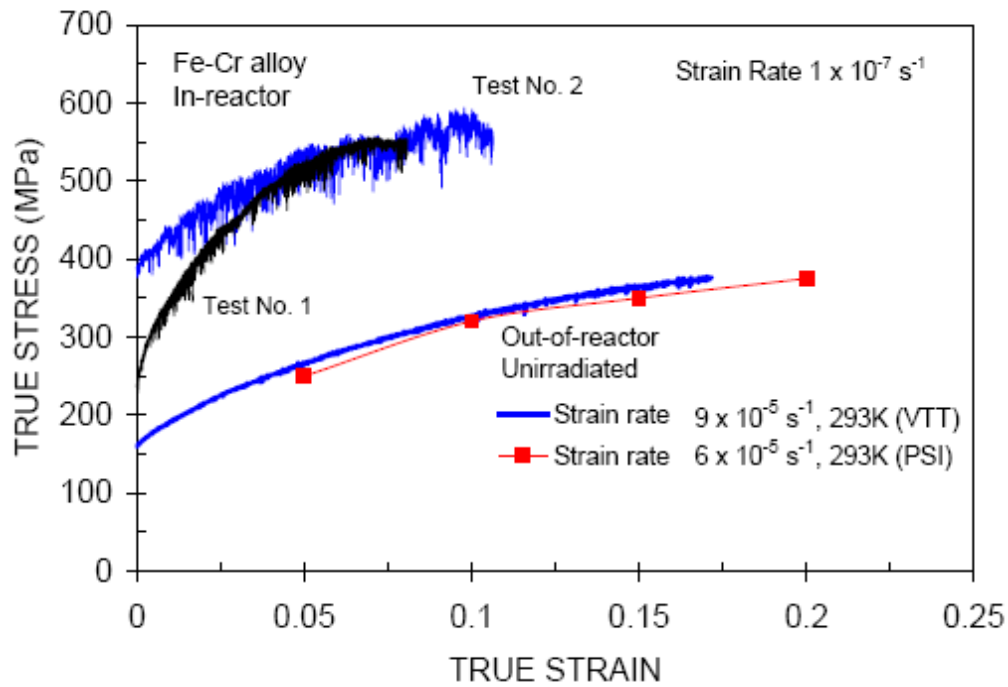


Figure 5. The conventional true stress-true strain curves for the in-reactor Test No. 1 and Test No. 2 carried out at a strain rate of $1.0 \times 10^{-7} \text{ s}^{-1}$ at 325 and 327 K, respectively. For comparison, the stress-strain curves for the unirradiated Fe-Cr-alloy tested at 293 K are also shown. Note that the out-of-reactor tests were carried at higher strain rates (indicated in the figure).

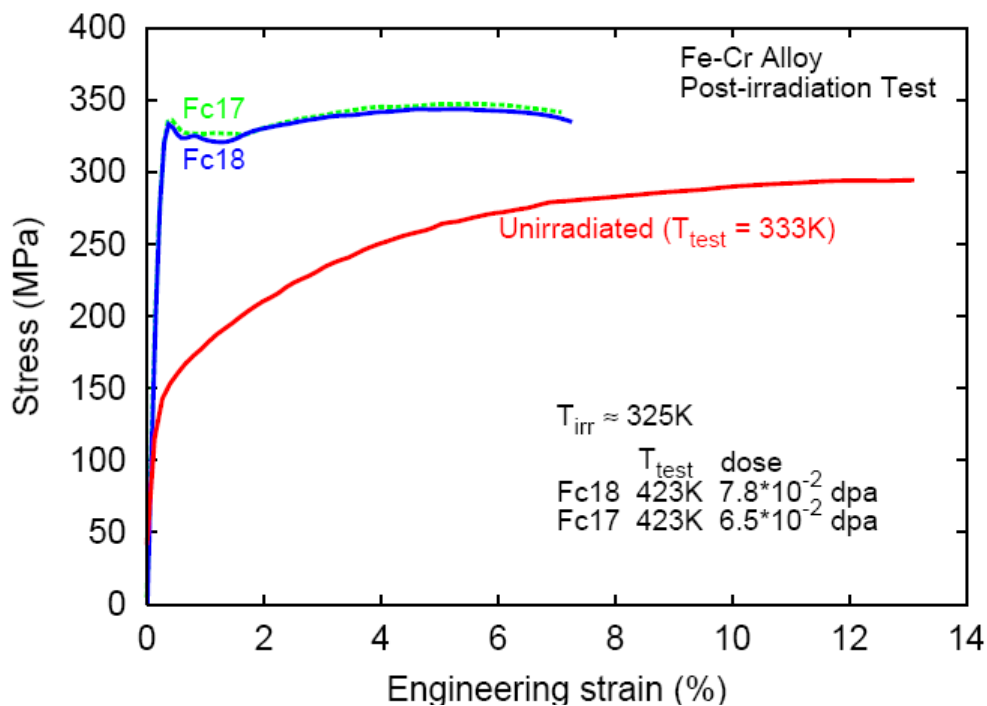


Figure 6. Engineering stress-strain curves for the Fe-Cr specimens post-irradiation tensile tested at 423 K with a strain rate of $1.3 \times 10^{-3} \text{ s}^{-1}$. The Fe-Cr specimens had received a displacement dose of 7.8×10^{-2} and 6.5×10^{-2} dpa at the irradiation temperature of 325 K. The stress-strain curve for the unirradiated Fe-Cr specimen tested at 333 K with a strain rate of $1.3 \times 10^{-3} \text{ s}^{-1}$ is also shown.

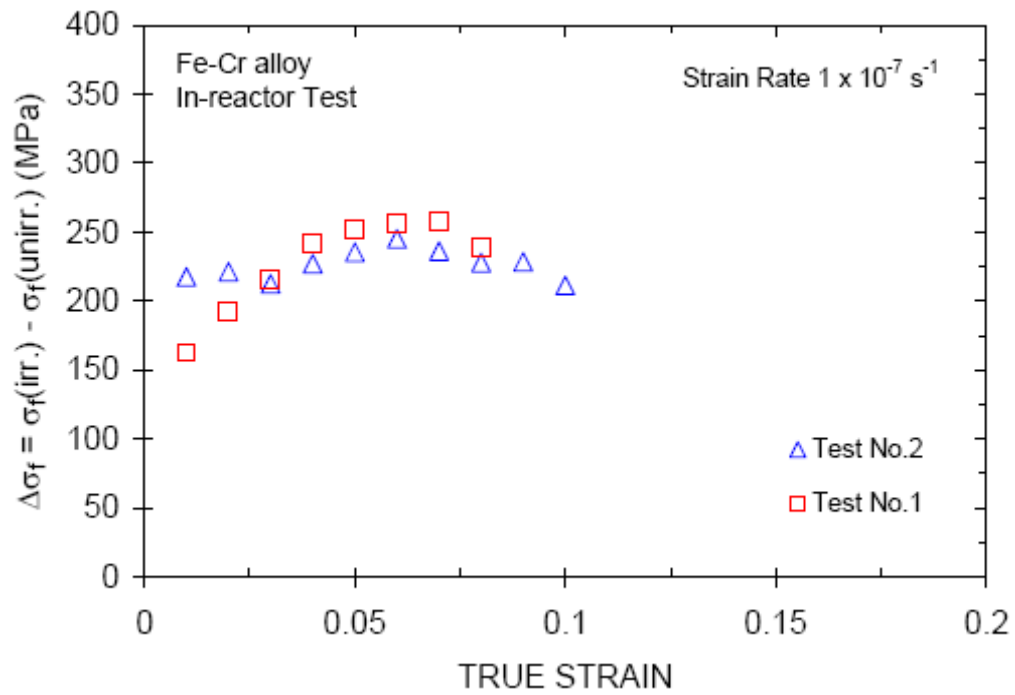


Figure 7. The variation of the increase in the post-yield flow stress due to irradiation, $\Delta\sigma_f$, as a function of true plastic strain for the in-reactor Test No. 1 and Test No. 2 on Fe-Cr specimens. Note that in the case of Test No. 2 on the specimen with a relatively high pre-yield dose of 1.1×10^{-2} dpa, the magnitude of the irradiation induced increase in the flow stress does not change much with increasing strain (dose).

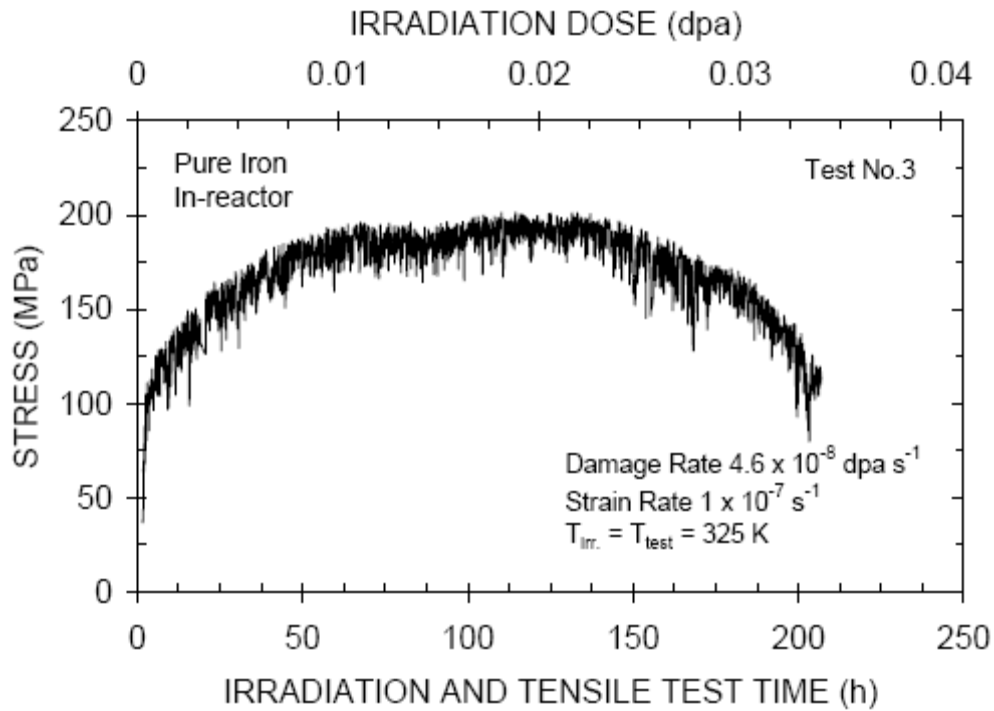


Figure 8. Continuously measured stress response of the pure iron specimen as a function of irradiation and tensile test time (i.e. displacement dose) during the in-reactor Test No. 3 with a pre-loading dose of 2.7×10^{-4} dpa. The pre-loading dose refers to the displacement dose that the specimen received before the actual tensile test was activated. The in-reactor test was carried out at 325 K with a strain rate of $1.0 \times 10^{-7} \text{ s}^{-1}$.

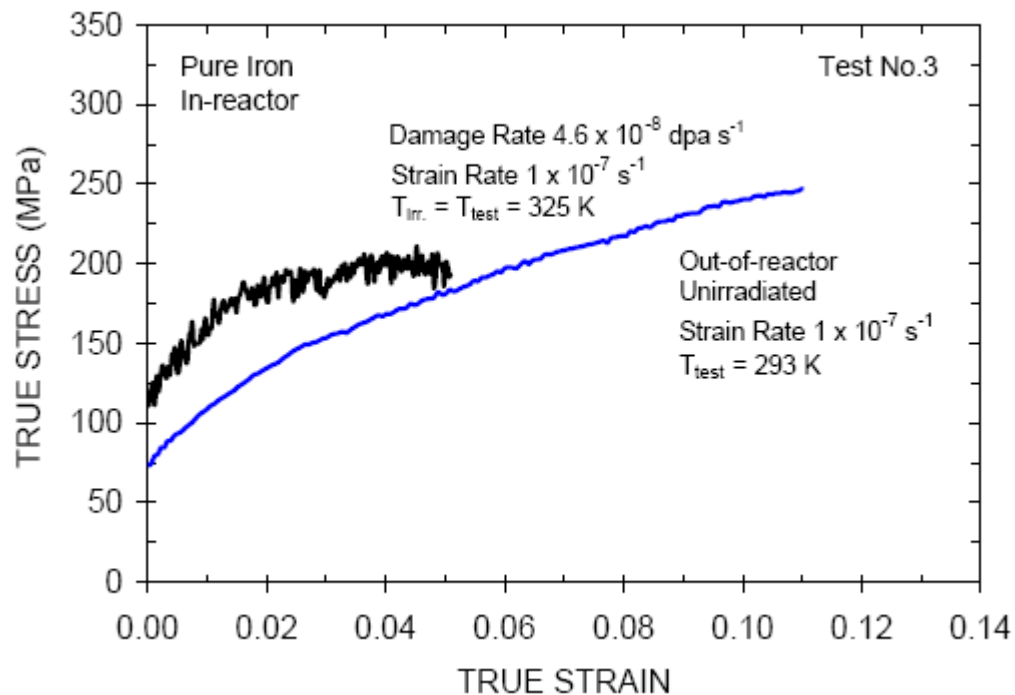


Figure 9. The conventional true stress-true strain curves for the in-reactor Test No. 3 carried out at 325 K with a strain rate of $1.0 \times 10^{-7} \text{ s}^{-1}$. For comparison, the stress-strain curve for the unirradiated reference specimen tested at 293 K with a strain rate of $1.0 \times 10^{-7} \text{ s}^{-1}$ is also shown.

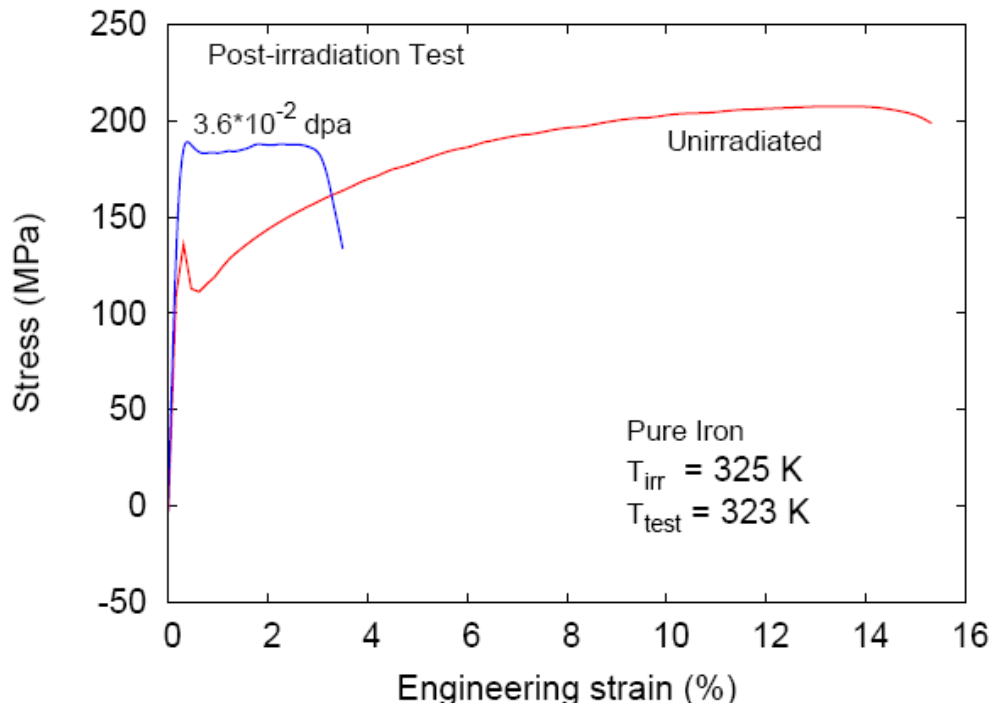


Figure 10. Engineering stress-strain curves for the iron specimen post-irradiation tensile tested at 323 K. The iron specimen had received a displacement dose of 3.6×10^{-2} dpa at 325 K. For comparison, the stress-strain curve for the unirradiated iron specimen tested at 323 K is also shown. Both the post-irradiation test and the test on the unirradiated iron specimens were carried out with a strain rate of $1.3 \times 10^{-3} \text{ s}^{-1}$.

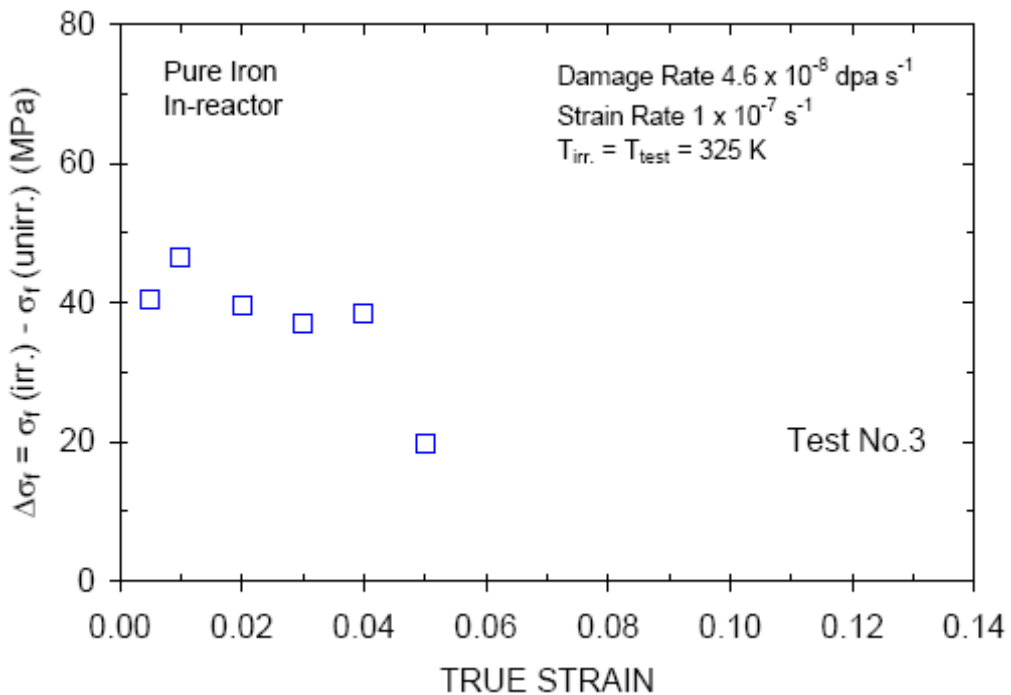


Figure 11. The variation of the increase in post-yield flow stress due to irradiation, $\Delta\sigma_f$, as a function of true plastic strain for the in-reactor Test No. 3 on pure iron specimen.

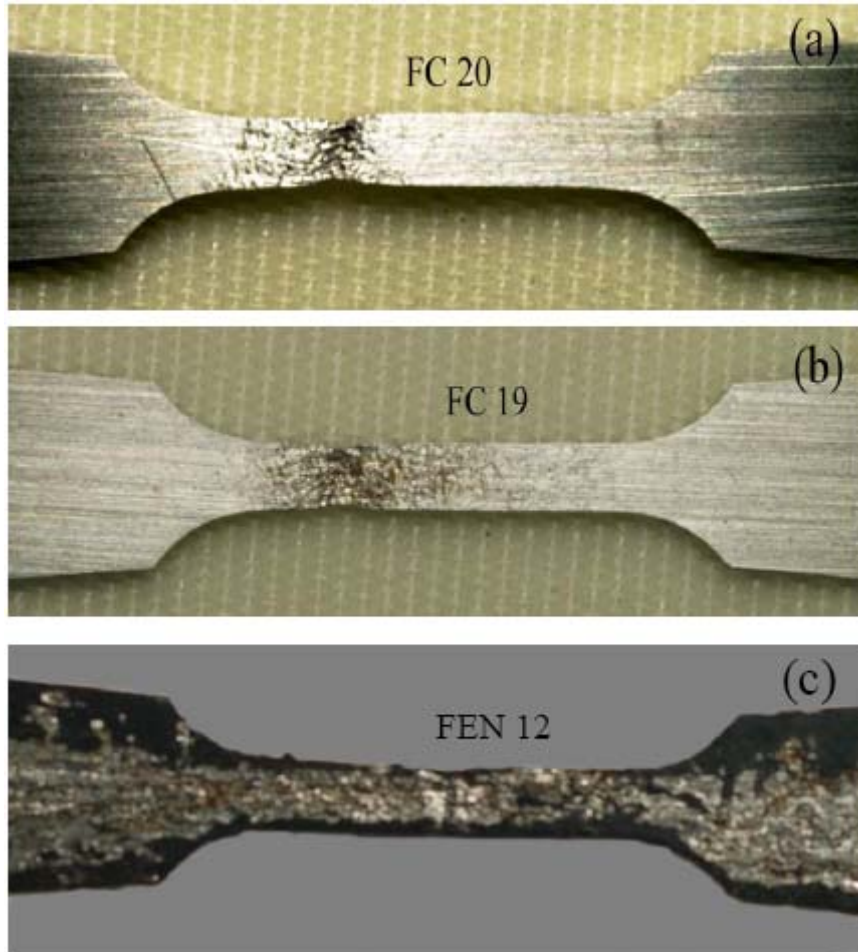


Figure 12. Photographs of tensile specimens of Fe-Cr and pure iron after the in-reactor (a) Test No. 1, (b) Test No. 2 and (c) Test No. 3. Note that the specimens in the Test No. 1, 2 and 3 had reached a total elongation of 12, 14.3 and 7.4 % (see Table 3), respectively, before the onset of fracture when the tests were stopped. The fracture zone is clearly visible in all three specimens.

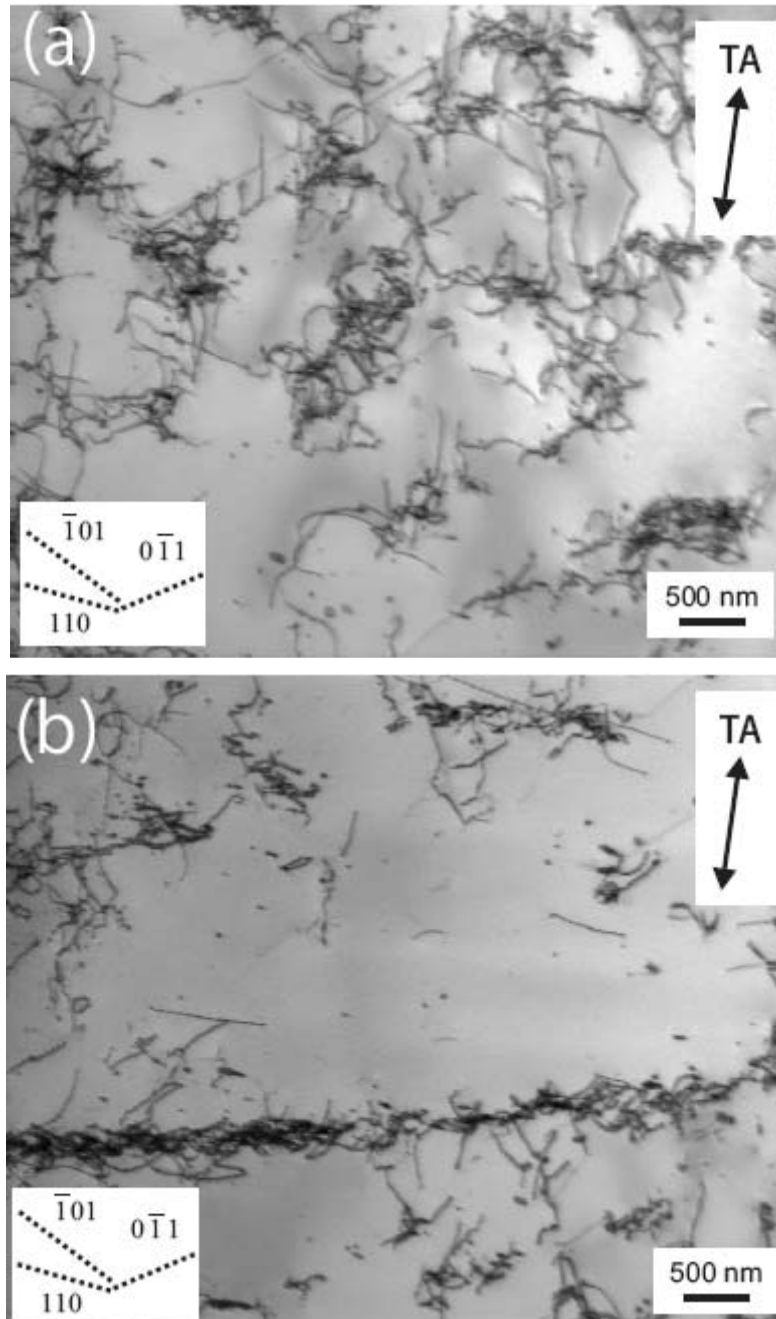


Figure 13. Dislocation microstructure in the unirradiated Fe-Cr specimen tensile tested at 333 K with a strain rate of $1.3 \times 10^{-3} \text{ s}^{-1}$ to a total strain level of 1.0 % showing (a) early stages of dislocation cell formation and (b) occasional formation of long dislocation walls.

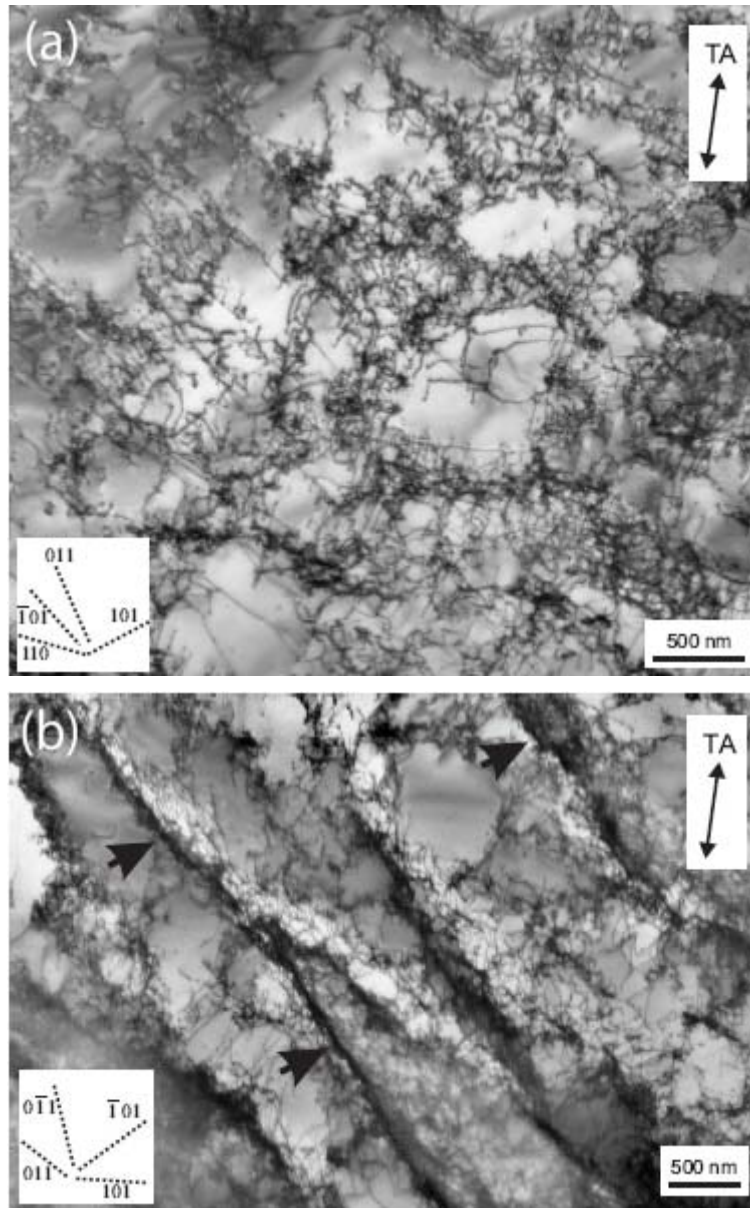


Figure 14. Same as in Figure 13 for Fe-Cr specimen tensile tested to a total strain level of 5 % showing (a) a typical cell structure with the cell boundaries of high dislocation density and the cell interiors almost free of dislocations and (b) long and dense dislocation walls (indicated by arrows) and loose cells between the walls.

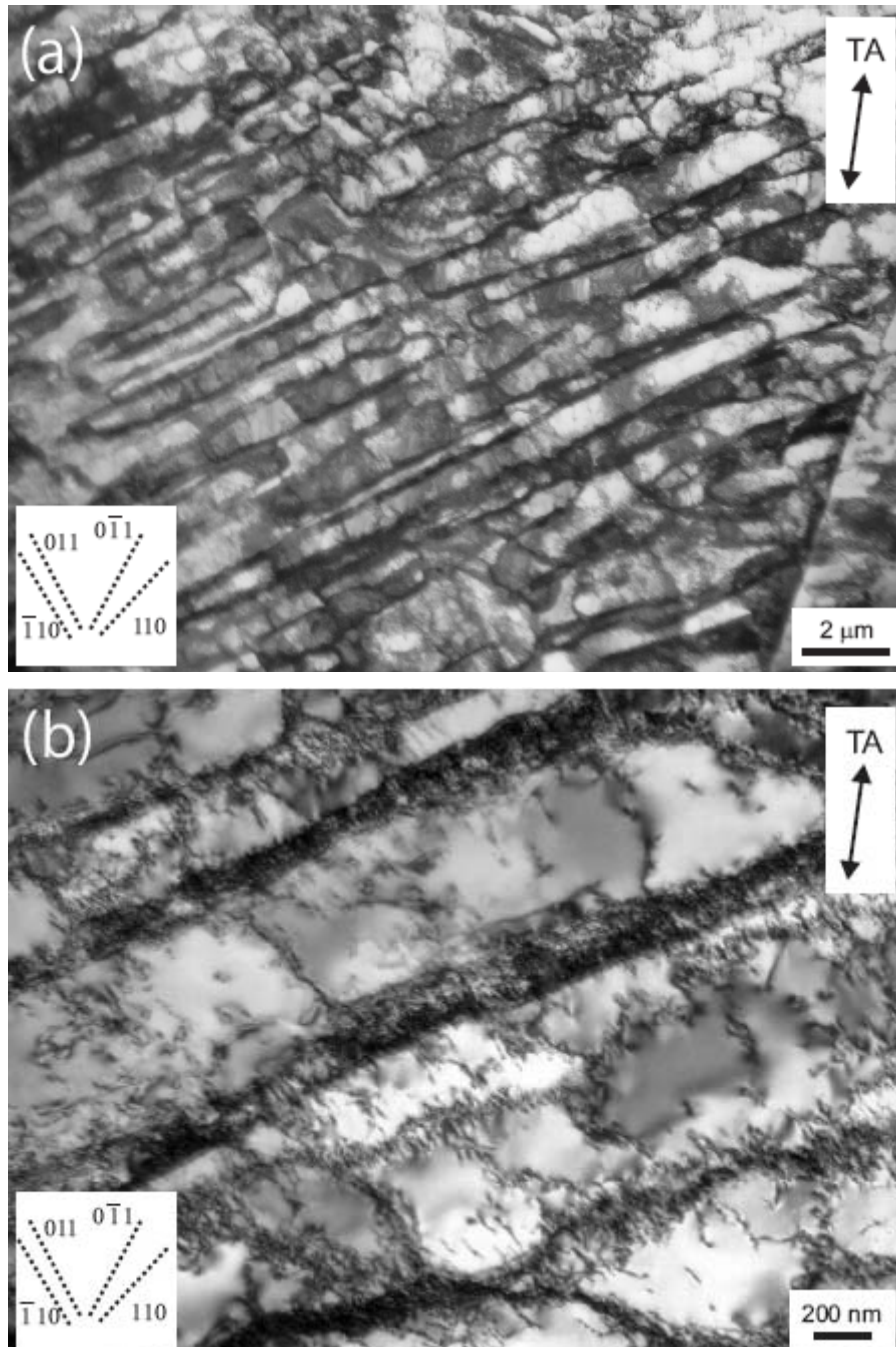


Figure 15. Same as in Figure 13 for Fe-Cr specimen tensile tested to a total strain level of 15 % showing (a) well developed dense and long dislocation walls formed at an angle of about -55° to the tensile axis and (b) dislocation cells between the dense dislocation walls.

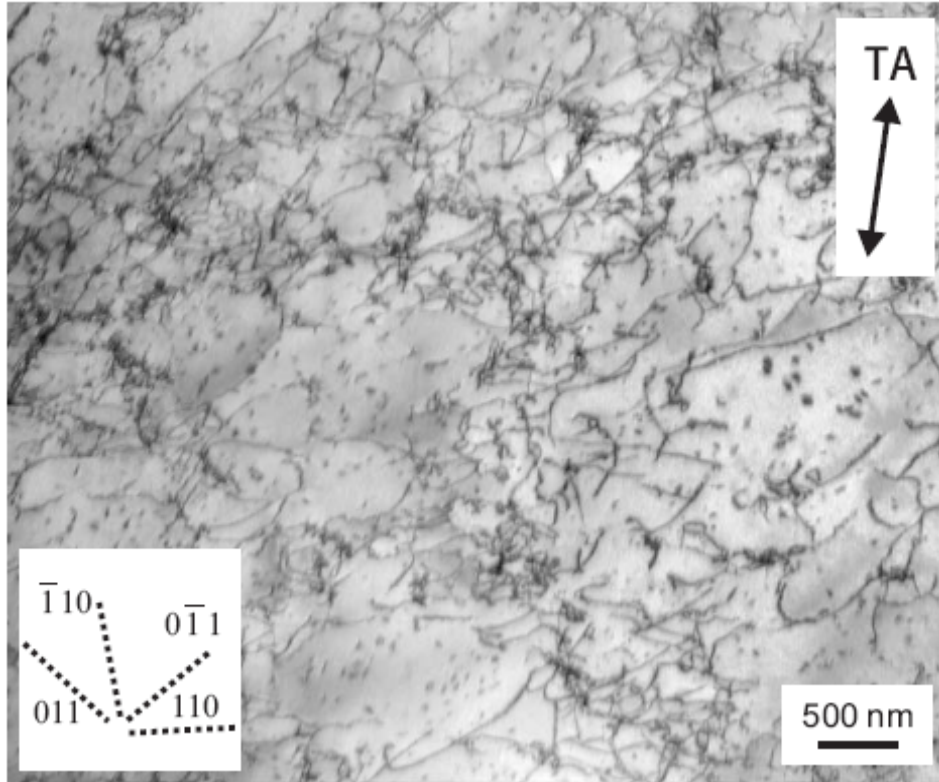


Figure 16. Dislocation microstructure in the uirradiated pure iron specimens tensile tested at 333 K with a strain rate of $1.3 \times 10^{-3} \text{ s}^{-1}$ to a total strain level of 1.0 % showing tendency for dislocation tangle formation. Note the absence of cell formation. Surprisingly, a large number of loops are formed during deformation.

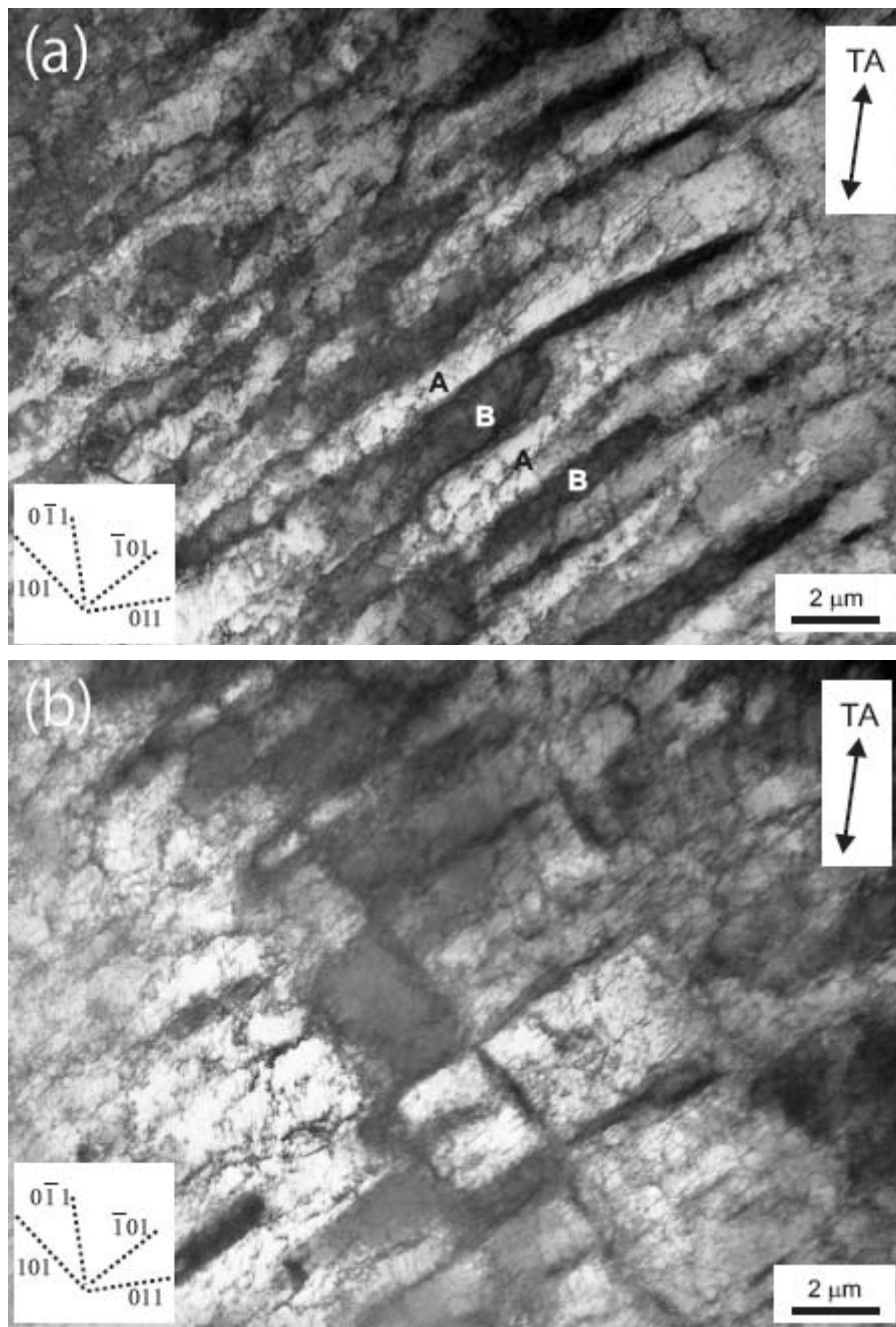


Figure 17. Same as in Figure 16 but for pure iron specimen tensile tested to a total strain level of 5.0 % showing (a) formation of one set of dense dislocation walls separating regions with alternating light (marked A) and dark (marked B) contrast indicating an alternating change in the misorientation between the regions and (b) formation of two sets of dense dislocation walls.

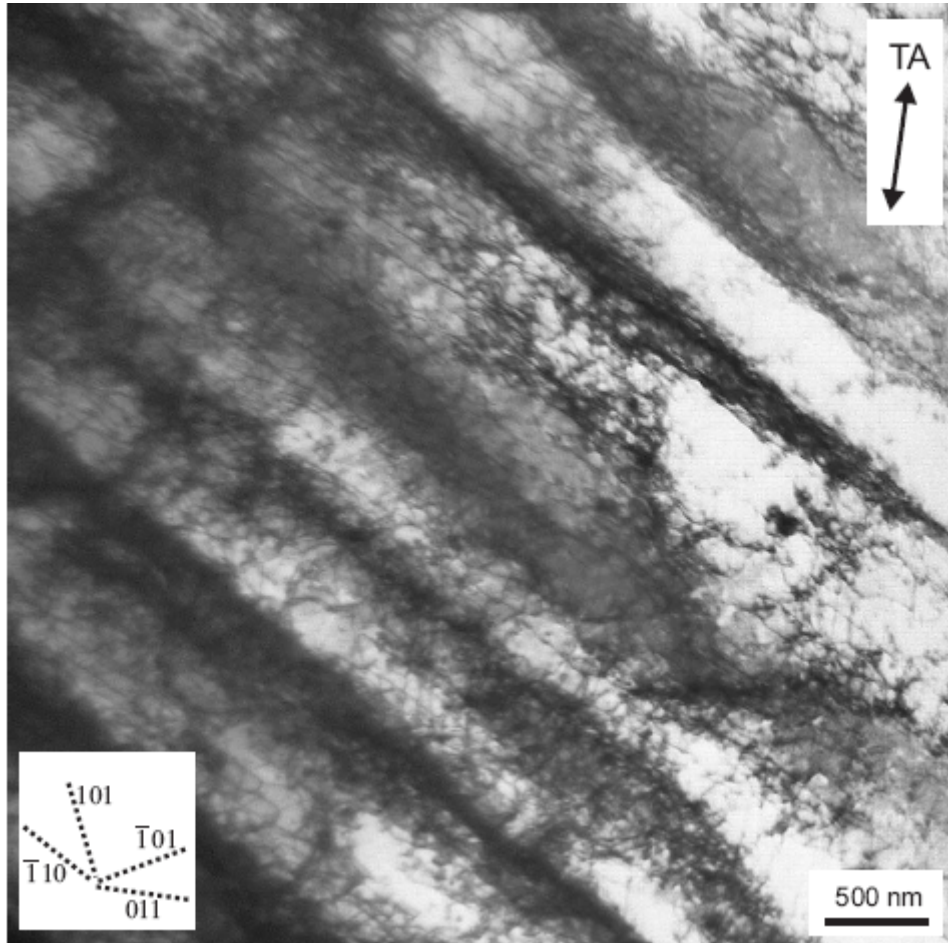


Figure 18. Same as in Figure 16 but for pure iron specimen tensile tested to a total strain level of 10 % showing the formation of dense dislocation walls parallel to $(\bar{1}10)$ trace and loose cells and dislocations in the volumes between the walls.

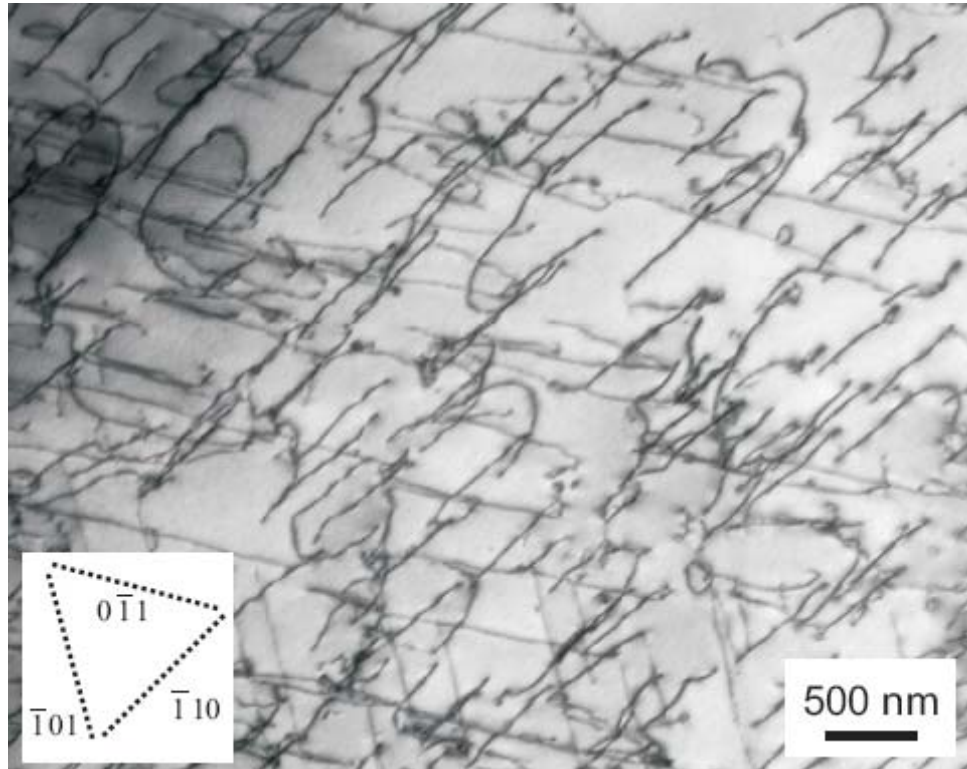


Figure 19. Dislocation microstructure in the Fe-Cr specimen (FC 20) used in the in-reactor Test No. 1 (see Figure 12 (a)) tensile tested at 325 K to a total strain level of 12.0 % (see Table 3) and to a dose level of 7.8×10^{-2} dpa (see Table 2) with a strain rate of $1.0 \times 10^{-7} \text{ s}^{-1}$ showing relatively low density of mostly straight dislocations with a homogeneous distribution. Note that the straight dislocations are parallel to the traces of the three $\{011\}$ planes (marked on the micrograph) lying in the $[111]$ zone axis.

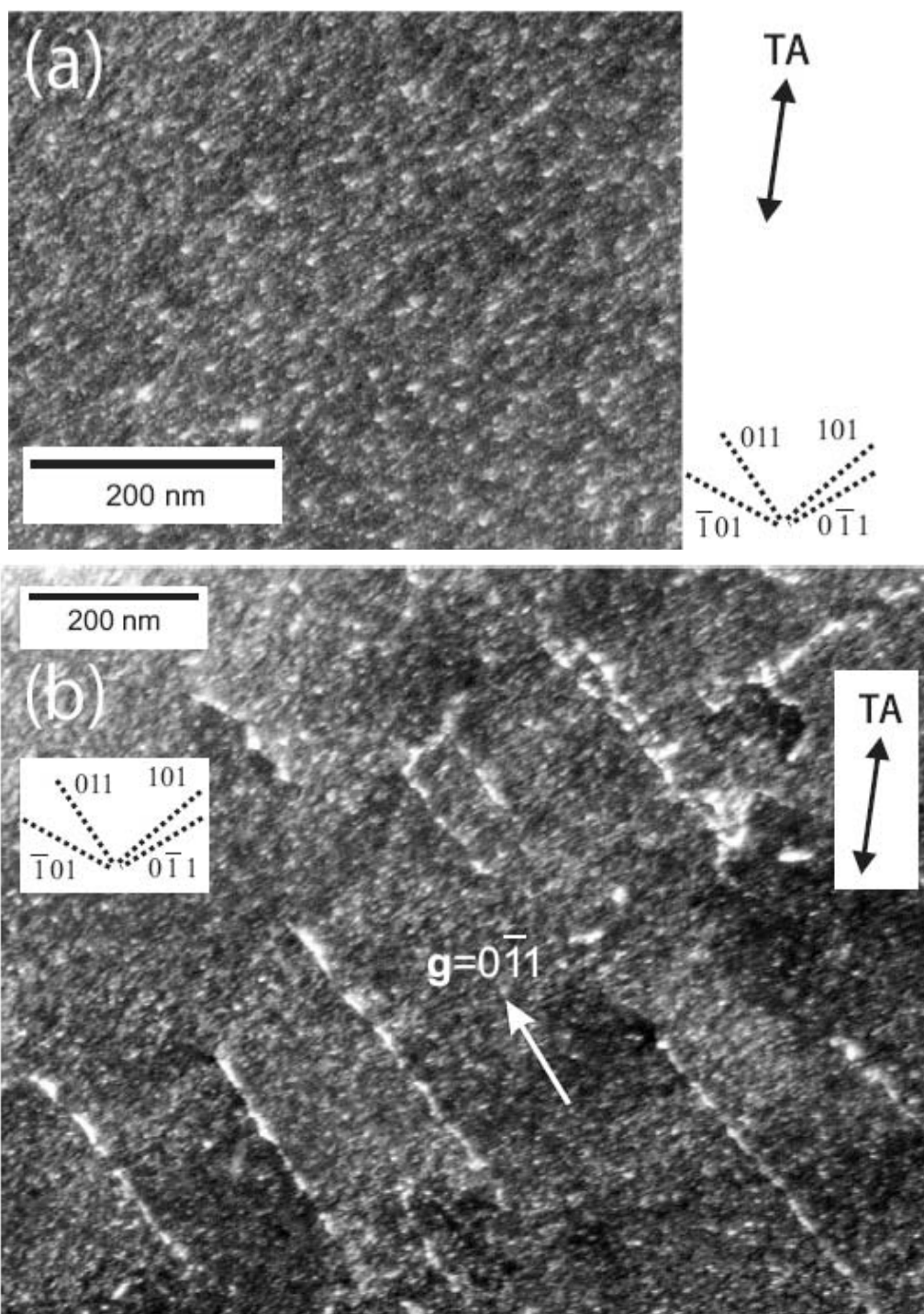
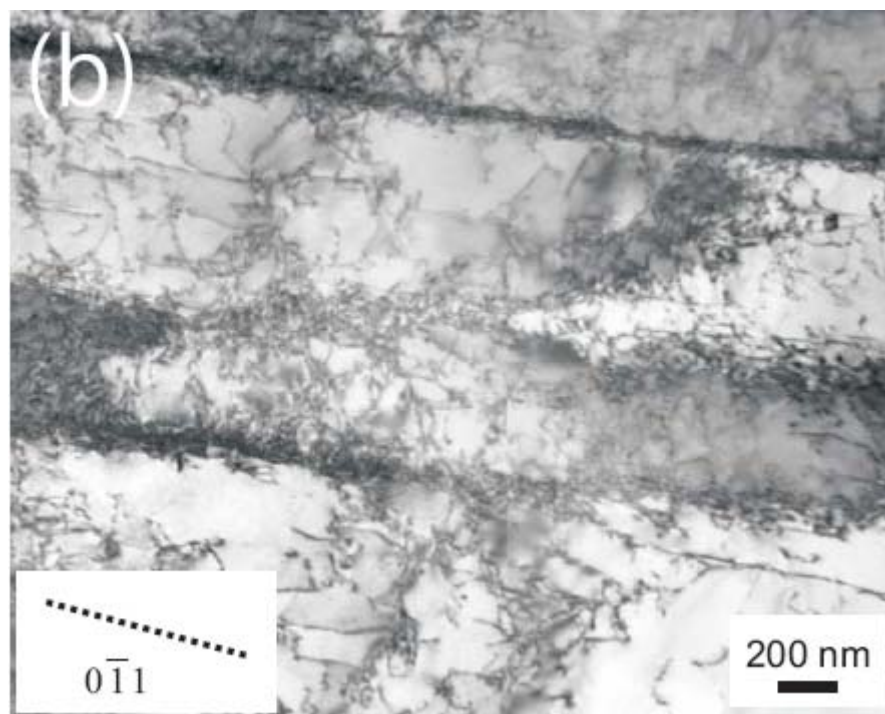
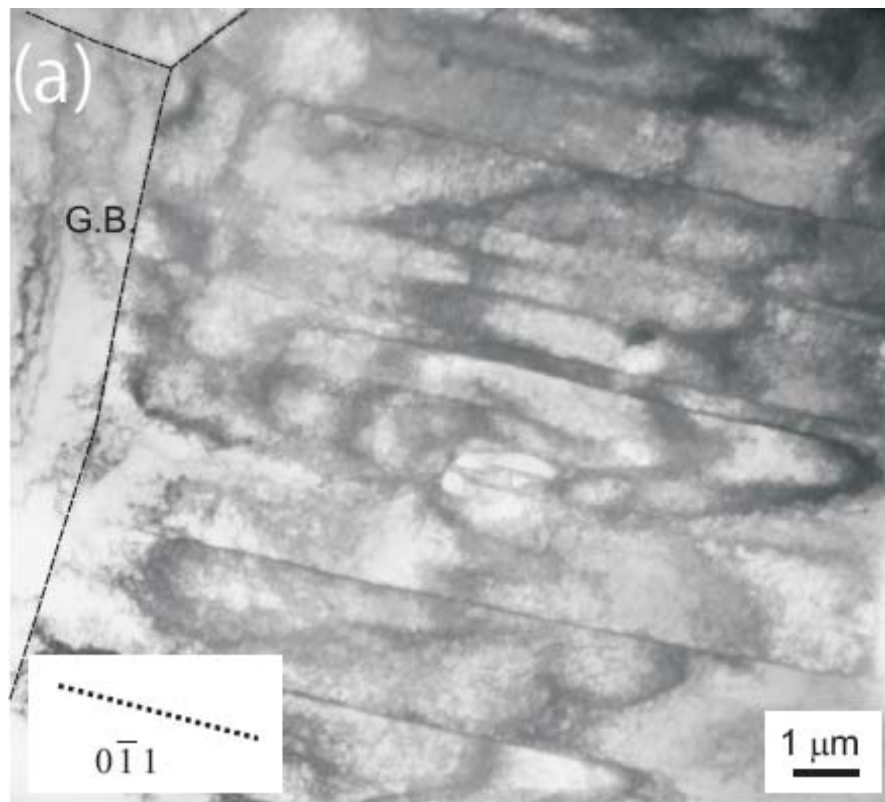


Figure 20(a). The weak beam dark field image illustrating the presence of very small defect clusters/loops in the Fe-Cr specimen used in the in-reactor Test No. 1. Note that the micrograph shown here was obtained from the same thin foil used for obtaining the dislocation microstructure shown in Figure 19. Figure 20(b) shows the defect clusters/loops in the same specimen that was used to obtain the microstructure shown in Figure 19 and 20 (a). Note that, the micrograph shows some straight dislocations that appear to be decorated with clusters.



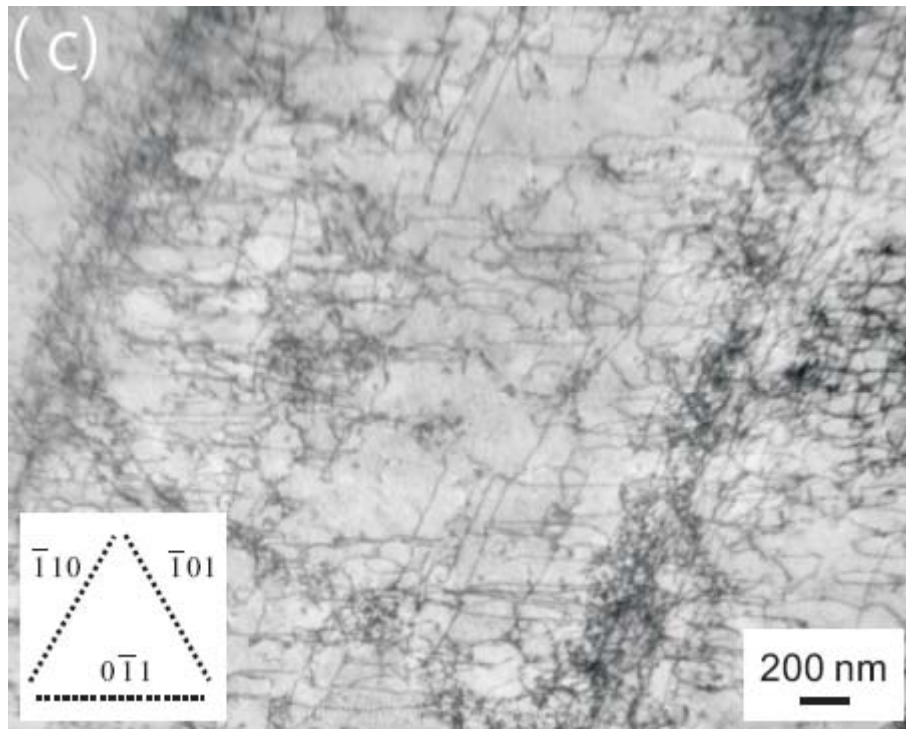
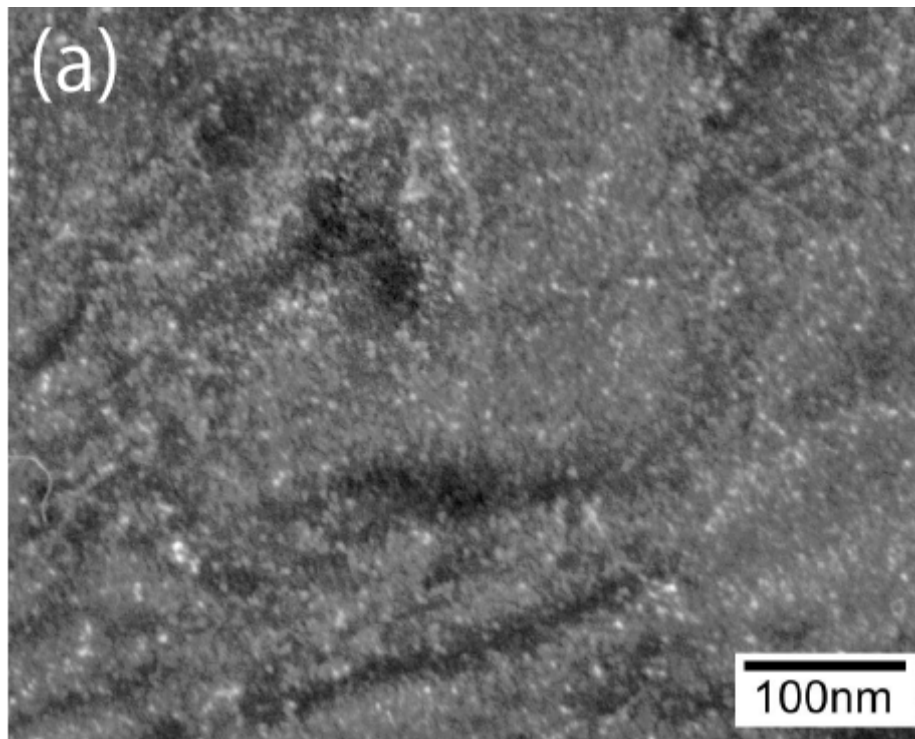


Figure 21. Dislocation microstructure in the Fe-Cr specimen (FC 19) used in the in-reactor Test No. 2 (see Figure 12 (b)) tensile tested at 327 K to a total strain level of 14.3 % (see Table 3) and to a dose level of 6.5×10^{-2} dpa (see Table 2)) with a strain rate of $1.0 \times 10^{-7} \text{ s}^{-1}$ showing (a) one set of extended dense dislocation walls approximately parallel to the trace of $(0\bar{1}1)$ plane, (b) dislocation tangles and loose dislocations in the volume between the walls and (c) almost straight dislocations between two dislocation walls.



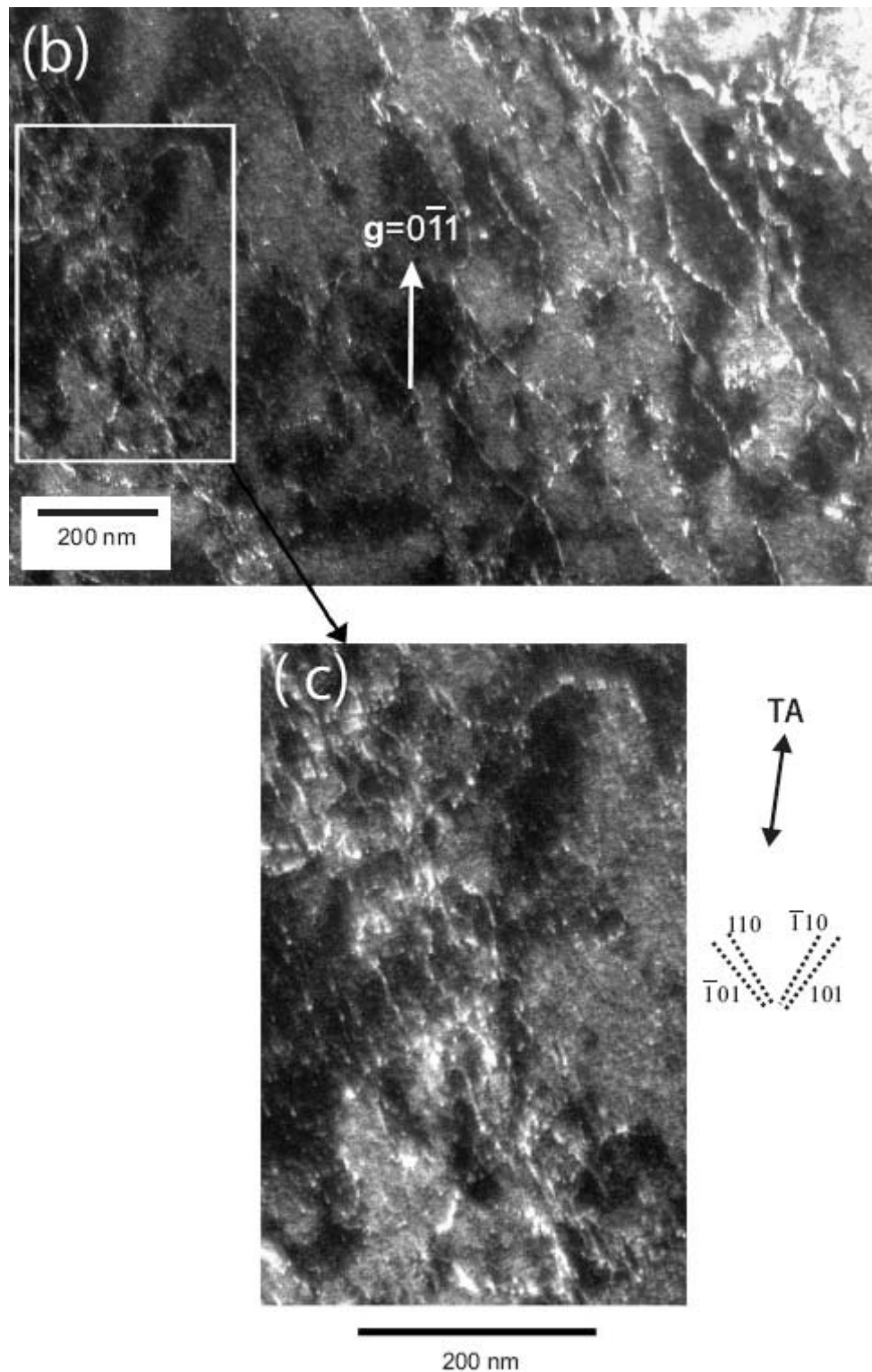


Figure 22. The weak beam dark field image (obtained from the same thin foil used for obtaining the dislocation microstructure shown in Figure 21) illustrating the presence of very small defect clusters/loops in the Fe-Cr specimen (a) away from the dislocation walls and (b) and (c) in the region containing dislocation walls. Note that dislocations in the walls are decorated with defect clusters and that the presence of dislocation walls makes the distribution of clusters heterogeneous and appears to reduce the density of clusters between the walls.

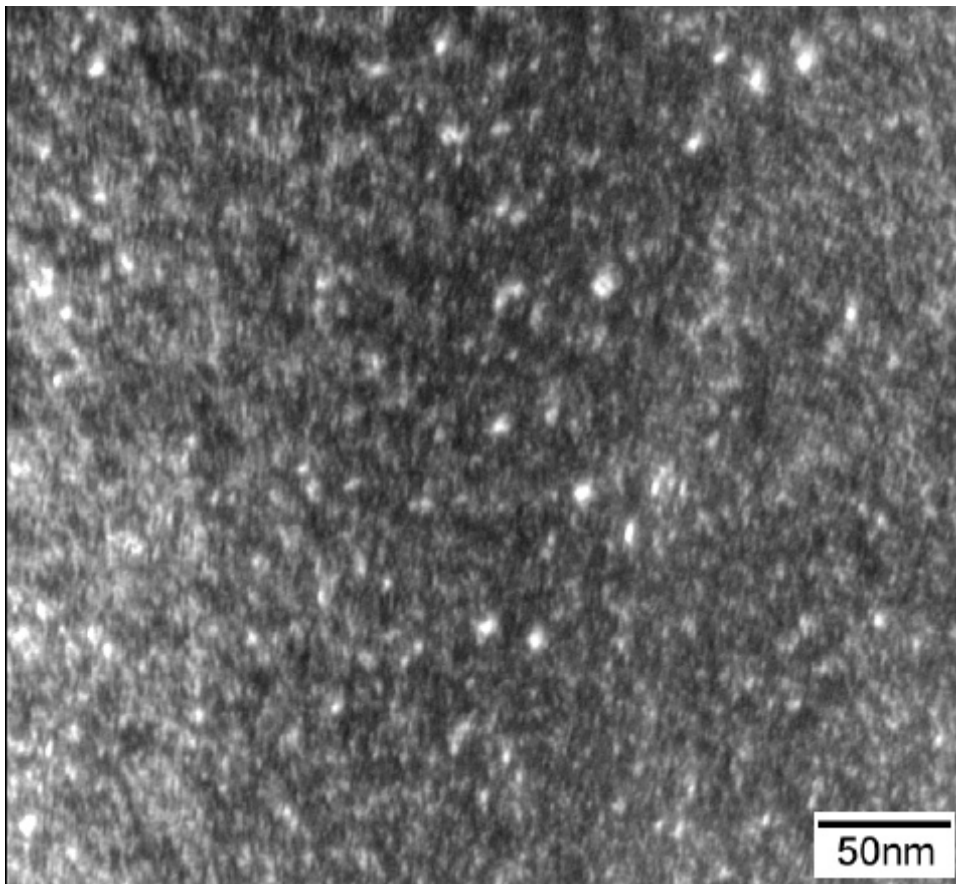
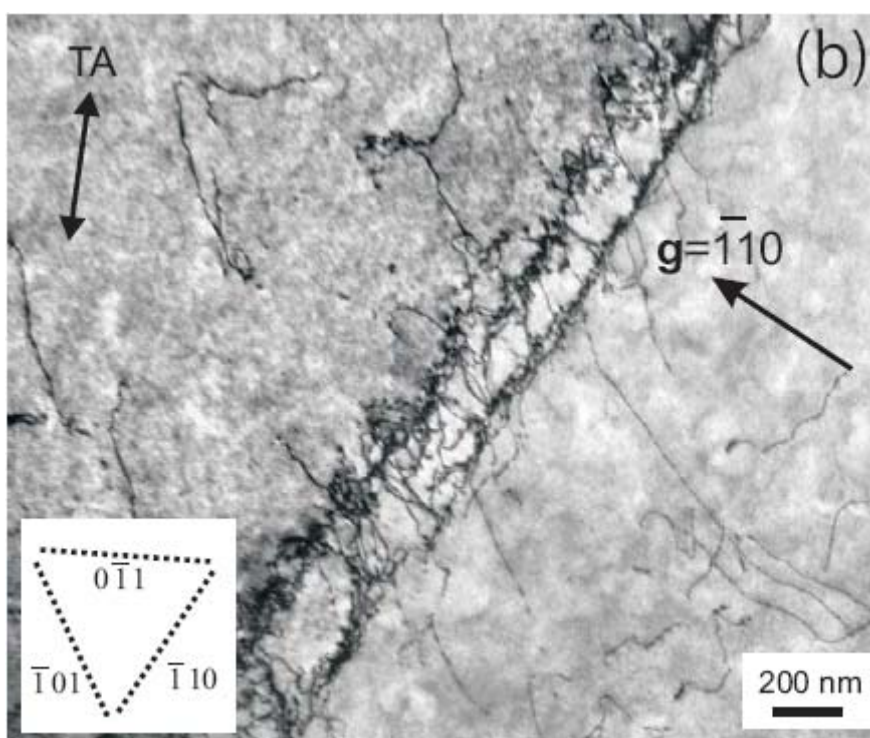
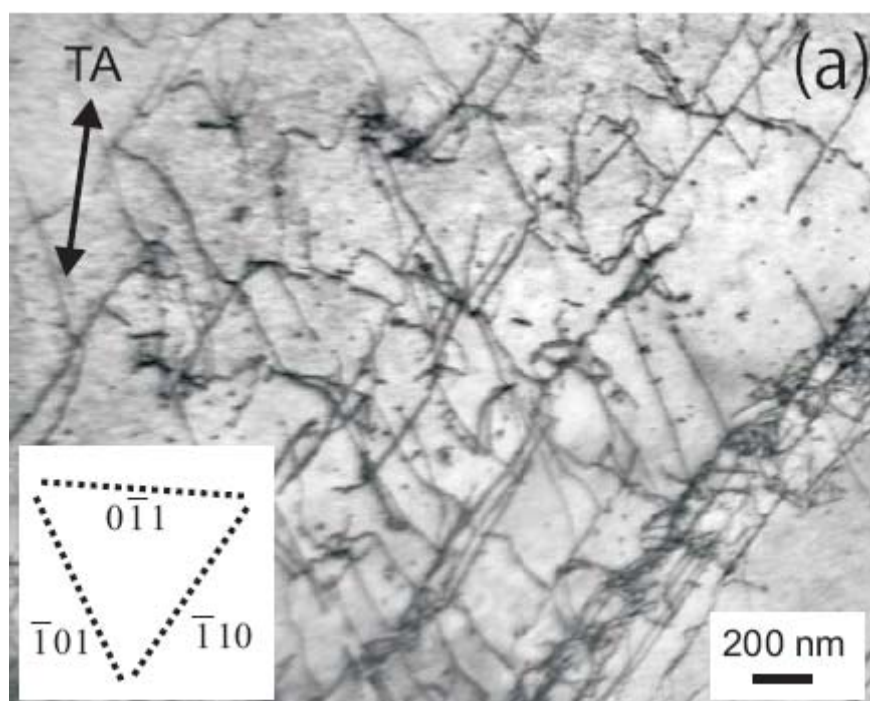


Figure 23. The weak beam dark field image of defect clusters in the underformed region of the Fe-Cr specimen tensile tested in the in-reactor Test No. 2 at 327 K to a displacement dose level of 6.5×10^{-2} dpa. Note a high density of homogeneously distributed small cluster/loops.



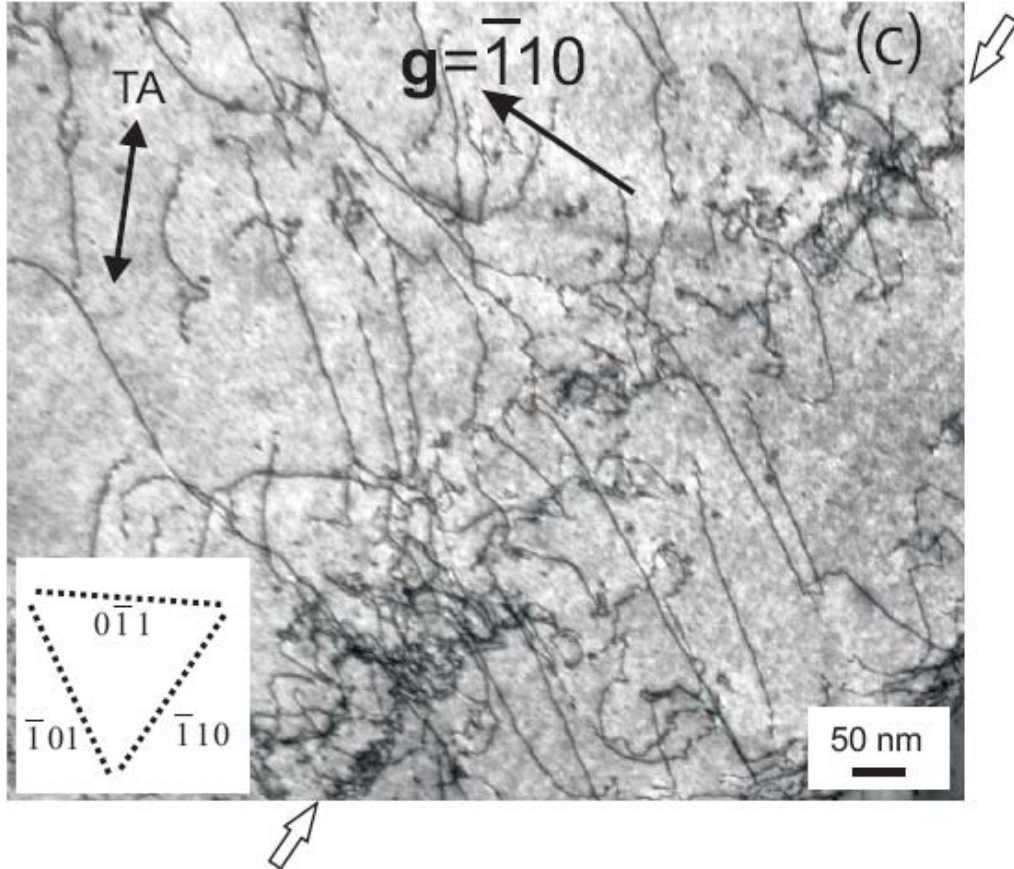


Figure 24. Dislocation microstructure in pure iron specimen (FEN 12) in-reactor tensile tested at 325 K (Test No. 3) to a total strain level of 7.4 % (see Table 3) and to a dose level of 3.5×10^{-2} dpa (see Table 2) with a strain rate of $1.0 \times 10^{-7} \text{ s}^{-1}$ showing (a) two sets of dislocations parallel to $(\bar{1}01)$ and $(\bar{1}10)$, (b) the formation of a microband in the $(\bar{1}10)$ plane and (c) the initiation of the formation of a weak microband along $(\bar{1}10)$ as indicated by two open arrows.

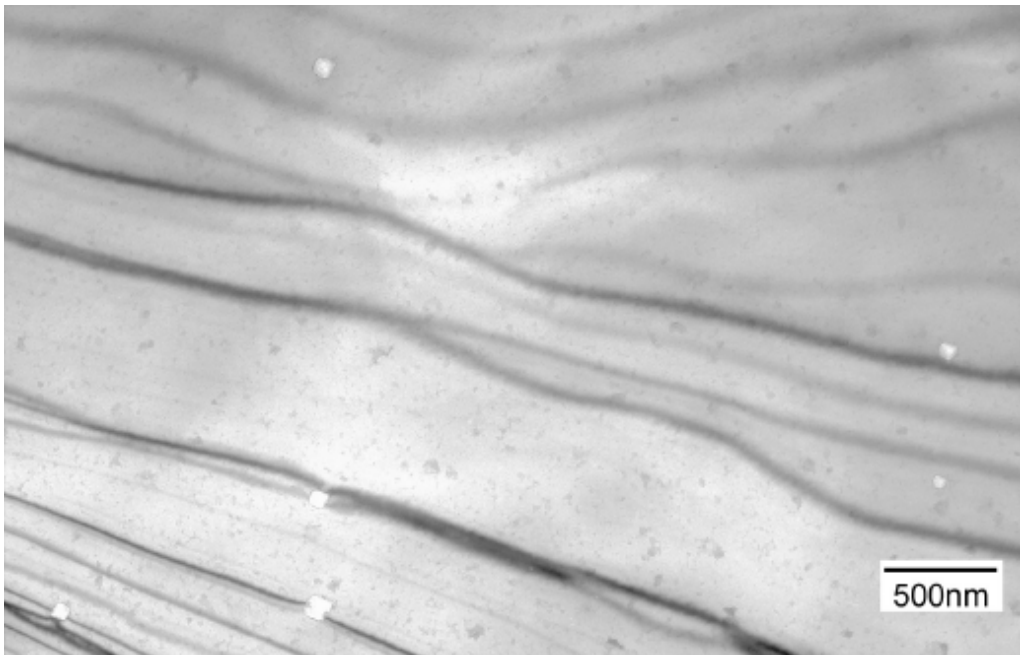


Figure 25. An example of voids formed in the undeformed region of the pure iron specimen used in the in-reactor Test No. 3. These large voids (~ 89 nm) were found to be present throughout the whole thin foil with a relatively low density ($\sim 1 \times 10^{19} \text{ m}^{-3}$).

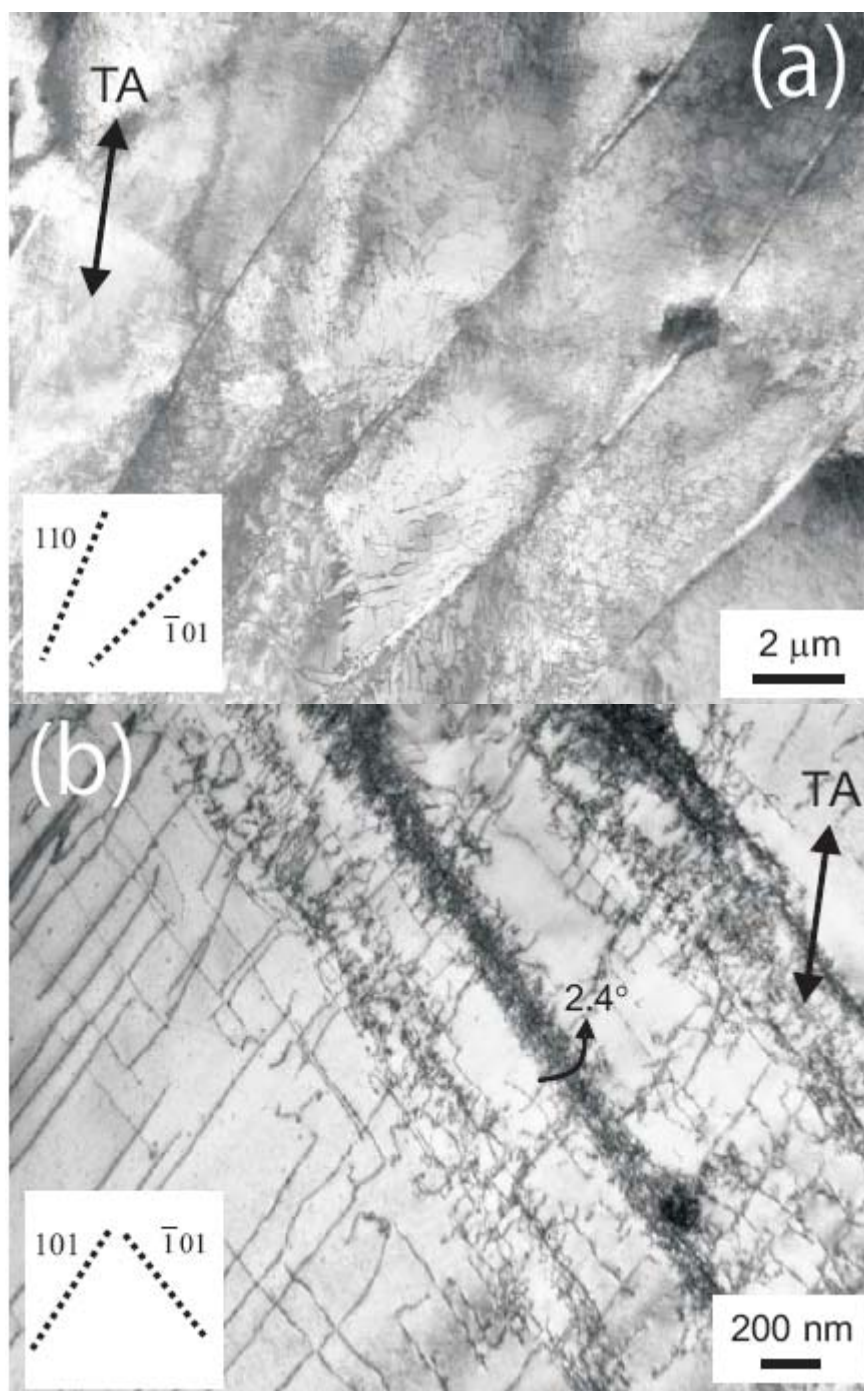


Figure 26. Microstructure in the Fe-Cr specimen post-irradiation tensile tested at 423 K. The specimen was irradiated (without any stress) at 327 K to a dose level of 6.5×10^{-2} dpa prior to post-irradiation tensile test carried out with a strain rate of $1.3 \times 10^{-3} \text{ s}^{-1}$. The microstructure illustrates the following: (a) formation of microbands extending over long distances ($>10 \mu\text{m}$) and (b) presence of long and straight dislocation lines and extended dense dislocation walls parallel to the ($\bar{1}01$) trace.

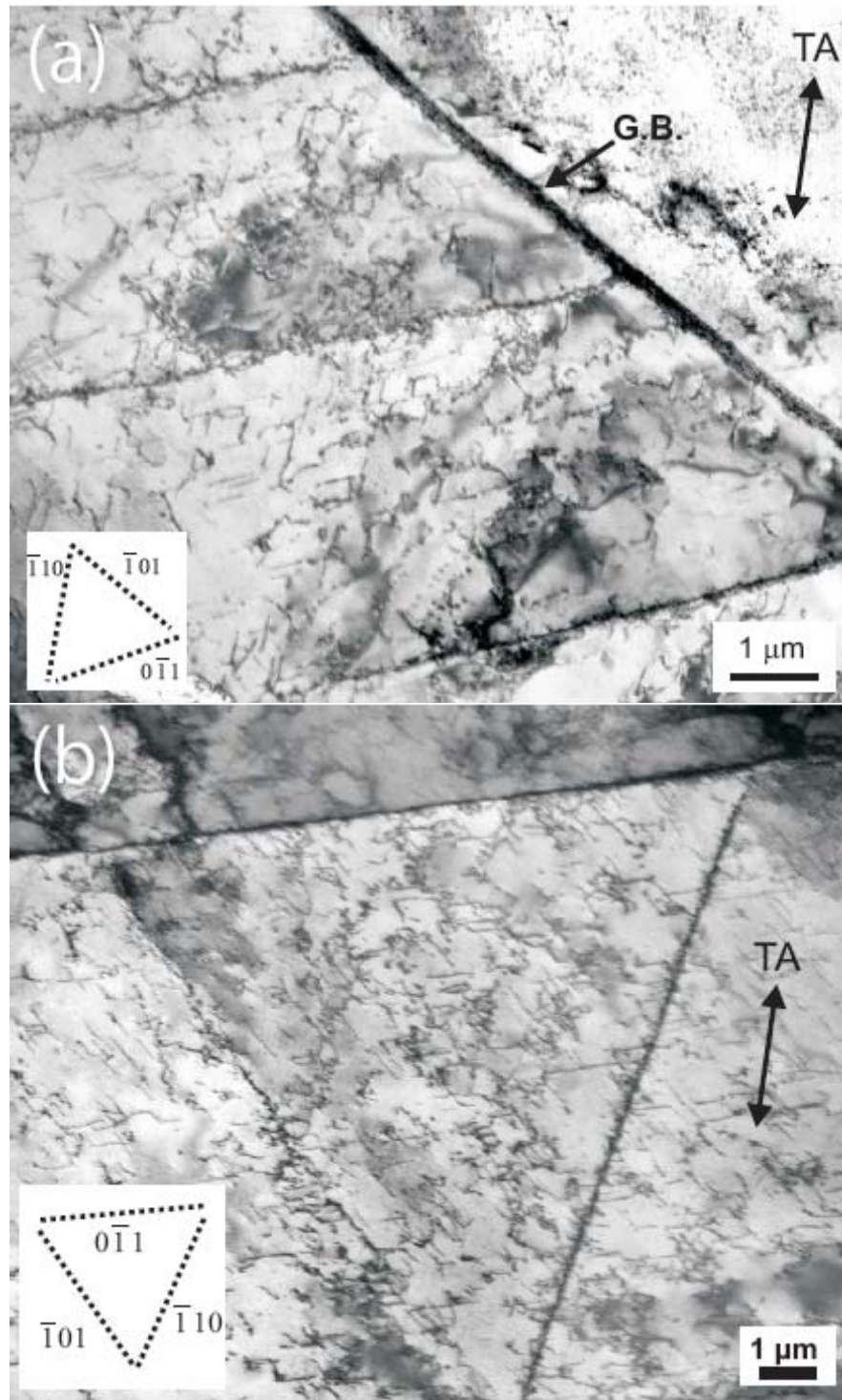


Figure 27. Microstructure in the pure iron specimen post-irradiation tensile tested at 323 K with a strain rate of $1.3 \times 10^{-3} \text{ s}^{-1}$. The specimen was irradiated (without any stress) at 325 K to a dose level of $3.6 \times 10^{-2} \text{ dpa}$. The microstructure illustrates the following: (a) formation of long dislocation walls parallel to the $(0\bar{1}1)$ plane ending at a grain boundary and three sets of dislocations parallel to the traces of three $\{110\}$ planes and (b) three sets of dislocation walls aligned with the three $\{110\}$ planes and three sets of dislocations parallel to the traces of the three $\{110\}$ planes.

Risø's research is aimed at solving concrete problems in the society.

Research targets are set through continuous dialogue with business, the political system and researchers.

The effects of our research are sustainable energy supply and new technology for the health sector.

